Published in final edited form as:
Nat Microbiol. 2021 August 01; 6(8): 981–990. doi:10.1038/s41564-021-00930-y.

Single-molecule imaging of LexA degradation in Escherichia coli elucidates regulatory mechanisms and heterogeneity of the SOS response

Emma C. Jones[1], **Stephan Uphoff**[1,*]

[1]Department of Biochemistry, University of Oxford, South Parks Road, Oxford, OX1 3QU, UK

Abstract

The bacterial SOS response stands as a paradigm of gene networks controlled by a master transcriptional regulator. Self-cleavage of the SOS repressor, LexA, induces a wide range of cell functions that are critical for survival and adaptation when bacteria experience stress conditions[1], including DNA repair[2], mutagenesis[3,4], horizontal gene transfer[5–7], filamentous growth, and the induction of bacterial toxins[8–12], toxin-antitoxin systems[13], virulence factors[6,14], and prophages[15–17]. SOS induction is also implicated in biofilm formation and antibiotic persistence[11,18–20]. Considering the fitness burden of these functions, it is surprising that the expression of LexA-regulated genes is highly variable across cells[10,21–23] and that cell subpopulations induce the SOS response spontaneously even in the absence of stress exposure[9,11,12,16,24,25]. Whether this reflects a population survival strategy or a regulatory inaccuracy is unclear, as are the mechanisms underlying SOS heterogeneity. Here, we developed a single-molecule imaging approach based on a HaloTag fusion to directly monitor LexA inside live *Escherichia coli* cells, demonstrating the existence of 3 main states of LexA: DNA-bound stationary molecules, free LexA and degraded LexA species. These analyses elucidate the mechanisms by which DNA-binding and degradation of LexA regulate the SOS response in vivo. We show that self-cleavage of LexA occurs frequently throughout the population during unperturbed growth, rather than being restricted to a subpopulation of cells, which causes substantial cell-to-cell variation in LexA abundances. LexA variability underlies SOS gene expression heterogeneity and triggers spontaneous SOS pulses, which enhance bacterial survival in anticipation of stress.

Gene expression heterogeneity can increase the odds of population survival under stress conditions by diversifying the behavior of individuals[26–28]. Distant bacterial species exhibit cell-to-cell heterogeneity in the SOS response, suggesting that it has a functional benefit[10,16,20,22,24] or that the accuracy of the conserved regulatory mechanism is inherently

*Correspondence to: stephan.uphoff@bioch.ox.ac.uk.

Author contributions

SU conceived the study. ECJ and SU generated and characterised cell strains. ECJ and SU performed single-molecule tracking experiments. SU performed microfluidic experiments. SU supervised the study and wrote the manuscript with input from ECJ.

Competing interests

The authors declare no conflict of interest.

Europe PMC Funders Author Manuscripts

limited[29,28]. Spontaneous SOS induction in a subpopulation of cells reduces the fitness costs of SOS gene expression for the population as a whole, while several studies suggest that it can increase short-term stress tolerance[18,30] and long-term evolutionary adaptation via SOS mutagenesis[5,31,32]. During interbacterial warfare, spontaneous SOS induction of bacteriocin toxins can serve as a pre-emptive attack strategy against a competing bacterial species[12]. Although spontaneous induction of prophages via the SOS response can be lethal for an individual host cell, it can lead to competitive advantages for the population[17,33]. Prophage induction and lysis of a subpopulation of cells promotes biofilm formation[11], horizontal gene transfer[6], and the release of phage-encoded toxins, such as *E. coli* Shiga toxin[8,9,33]. Nevertheless, the underlying molecular mechanisms responsible for the heterogeneity and spontaneous induction of the SOS response remain incompletely understood.

Single-cell measurements of the SOS response have relied entirely on fluorescent gene expression reporters[4,10,16,21–25], but the output of these reporters is itself confounded by gene expression noise that is difficult to distinguish from genuine cell-to-cell variation in SOS signalling[34]. Moreover, cellular stress causes global physiological changes that affect the output of gene expression reporters independently of the SOS response, and several SOS genes are co-regulated by other stress responses[35,36]. Although SOS signalling can be measured directly using immunoblots that detect the cleavage of LexA[37], these assays cannot monitor SOS response dynamics at a single-cell level. As such, it is unknown how heterogeneity in the SOS outputs relates to the underlying input from LexA. Furthermore, key functions of LexA and regulatory mechanisms of the SOS response have been inferred using indirect genetic methods or *in vitro* biochemical assays, but not been observed directly *in vivo*.

This motivated the development of a microscopy-based approach for visualising LexA function in individual living cells. We replaced the endogenous *lexA* gene with a HaloTag fusion allowing covalent labelling with the cell-permeable fluorophore Tetramethylrhodamine (TMR) (Fig. 1a). Cells expressing LexA-Halo exhibit normal growth, viability, SOS gene repression, and survival during treatment with DNA damaging agents (Extended Data Figs. 1–2). UV resistance was mildly perturbed, but far less so than for SOS response-deficient mutant strains (Extended Data Fig. 1). These and other characterisations (see Materials and Methods) show that the LexA-Halo fusion closely recapitulates native LexA function. High-speed single-molecule imaging (7 ms/frame) on a custom-built microscope[38] and reversible photoswitching of TMR[39] allowed us to record hundreds of tracks of LexA-Halo molecules per cell (Fig. 1b). During normal growth, cells showed a distinct population of immobile LexA molecules (P_{bound} = 4.8±0.4 % of tracks with D ~ 0.1 μm^2/s) and a mixture of mobile LexA species with a broad range of diffusion coefficients from D = 0.2 to 12 μm^2/s (Fig. 1c). The abundance of LexA has been estimated to 600 – 1300 molecules/cell[37,40,41]. Based on this, the population of immobile LexA molecules is in the range of ~14 – 31 LexA dimers. This is consistent with the number of LexA dimers required to repress ~40 genes in the SOS regulon considering that many of these genes are not fully repressed during normal growth (e.g. *lexA*, *recA*, *uvrA*, etc)[2]. To test if immobile molecules are indeed DNA-bound, we examined LexAE71K and LexAE45K mutants that have increased DNA-binding affinity and reduced promoter specificity, respectively[42,43]. Because *lexA* transcription is auto-regulated, we expressed mutants from an ectopic pBAD

promoter in a Δ*lexA* strain, thus ensuring that expression levels are equal for different variants. As predicted, LexAE71K and LexAE45K both exhibited a larger population of immobile molecules compared to wild-type LexA (Fig. 1d). The E45K mutation also decreased the diffusion coefficients of the mobile LexA population, consistent with a loss of promoter specificity and an increased frequency of transient non-specific DNA interactions[42,44]. To probe specific binding of LexA to SOS boxes, we transformed cells with pUC19 plasmids carrying promoters that are regulated by LexA, or the constitutive PpolA promoter as a negative control. Indeed, the bound LexA population increased in the presence of additional PdinG and PsulA promoters that contain one SOS box, and further increased for PrecN promoters with three SOS boxes (Fig. 1e).

The SOS response is triggered when RecA proteins form nucleoprotein filaments on single-stranded DNA at DNA breaks or stalled replication forks. Interaction of LexA with RecA filaments stabilises a conformation that causes LexA to cleave itself[45], which should separate the fluorescently-labelled C-terminal domain (LexA$^{85-202}$-Halo) from the N-terminal DNA-binding domain in our construct (Fig. 1a). Indeed, LexA-Halo mobility increased following a UV pulse due to a loss of DNA-bound and slowly diffusing molecules accompanied by the gradual appearance of a rapidly-diffusing population (Fig. 2a). The localization of LexA in untreated cells reflected the shape of the bacterial nucleoid. This organization was lost after UV exposure (Extended Data Fig. 3). LexA self-cleavage exposes recognition motifs for degradation of the protein fragments by Lon[46] and ClpXP proteases[47]. The distribution of diffusion coefficients of LexA-Halo 180 min post UV exposure was identical to that obtained from untreated cells expressing unconjugated HaloTag (Fig. 2b). Hence, the free HaloTag appears to remain in cells as a rapidly-diffusing species after degradation of the LexA$^{85-202}$ cleavage fragment. This is consistent with the inability of ClpXP to degrade the HaloTag from its N-terminus[48]. Detection of LexA species via SDS-PAGE and in-gel TMR fluorescence confirmed the UV-induced cleavage of LexA-Halo and its conversion into the free HaloTag (Fig. 2c). Hence, the presence of the rapidly-diffusing HaloTag can serve as a direct reporter for LexA degradation in live cells. Although LexA-Halo diffusion increased after UV treatment in a Δ*clpX* Δ*lon* strain with similar kinetics as in the wild-type, the average diffusion coefficients were lower throughout the response (Fig. 2d, Extended Data Fig. 4). This is consistent with the protease-deficient cells being unable to degrade the cleaved LexA$^{85-202}$-Halo fragment, which has a larger size and thus a lower mobility than the HaloTag alone.

The relative abundances of the DNA-bound population (P_{bound}), free LexA pool (P_{free}), and degraded LexA species ($P_{degraded}$) provide a quantitative readout for the progression of the SOS response in live cells (Extended Data Figs. 5–6). P_{free} decayed exponentially with a half-life of 19 min after 50 J/m^2 UV (16–27 min 95% CI), while lower UV doses caused slower and incomplete LexA degradation, as expected[37,49] (Fig. 2e). To study the role of LexA dimerization, we examined the G124D mutation that causes a 50-fold reduction in dimerization affinity[45]. The increased mobility of this mutant relative to the wild-type confirms that LexA is predominately dimeric in cells[45,50,51] (Fig. 2f). As dimerization is important for promoter recognition, the G124D mutation also diminished the DNA-bound population (Fig. 2f). Self-cleavage of LexA dimers is thought to occur separately for each

monomer[45,51]. In fact, we found that UV-induced degradation of monomeric LexAG124D proceeded faster than the wild-type (Fig. 2f).

Although LexA degradation induces an entire gene network, the activation times of different genes follow a specific chronology in response to DNA damage[2,52]. DNA repair genes are activated rapidly, whereas mutagenic DNA polymerases, toxins, and other factors with a burden on cell fitness or genome stability become induced later in the response as a strategy of "last resort"[2,3]. The differential gene induction is attributed to DNA-bound LexA being protected from self-cleavage[51], so that the activation time of each gene is governed by the dissociation rate constant of LexA from its promoter. Our data are consistent with this model. First, the decay of the DNA-bound population was slower than the decay of the free LexA pool (Extended Data Fig. 6b,c). Second, increasing the number of DNA-binding sites in cells protected the bound LexA population from degradation after UV treatment (Fig. 2g). Third, the population of bound LexA molecules resistant to degradation was higher in the presence of additional PsulA promoter sequences as compared to PdinG sequences, consistent with the delayed induction of *sulA* compared to *dinG* during the SOS response[2,52] (Fig. 2g). As expected, the degradation kinetics of the free LexA pool were unaffected by the presence of additional DNA-binding sites (Extended Data Fig. 6d-f). Together, single-molecule tracking of LexA-Halo confirms the key regulatory mechanisms of the SOS response *in vivo* (Fig. 2h).

Quantifying LexA populations in untreated cells via single-molecule tracking or in-gel fluorescence showed that a surprisingly large proportion of LexA molecules become degraded spontaneously during normal growth both for endogenous and pBAD-expressed LexA-Halo ($P_{degraded}$ = 32.0±2.6% and 30.0±1.6% respectively) (Fig. 3a-b). Bona-fide LexA self-cleavage is responsible for this, as degradation was diminished for the non-cleavable LexAK156A mutant[45] (Fig. 3a-b, Extended Data Fig. 7). Perturbed DNA replication and frequent DNA breakage in a Δ*dam* strain[53] strongly increased $P_{degraded}$ (Fig. 3a, Extended Data Fig. 7). However, inactivation of RecA did not abolish LexA degradation completely (Fig. 3a-b, Extended Data Fig. 7), demonstrating that DNA damage is not the sole trigger for cleavage. LexA is capable of adopting its auto-cleavable conformation without RecA co-protease[47,54–56], but the relevance of this pathway inside cells remained uncertain. The LexA V82S mutation has been shown to block auto-cleavage without perturbing RecA-dependent cleavage[54]. Indeed, $P_{degraded}$ was reduced for this mutant (Fig. 3a-b, Extended Data Fig. 7), showing that auto-cleavage contributes to a basal rate of LexA degradation.

Degradation of LexA during normal growth could be an underlying cause for spontaneous inductions of the SOS response which may function as a strategy of stress-anticipation in a subpopulation of cells[10,12,21,22,24,25]. Quantification of LexA populations in single cells revealed substantial cellular heterogeneity (Fig. 3a-d, Extended Data Fig. 8). The broad distributions of $P_{degraded}$ and P_{free} show that degradation is triggered very frequently, and not solely in a small subpopulation of cells as had been inferred from gene expression reporters[10,11,21,22,24,25]. Heterogeneity in the free LexA pool was further increased among Δ*dam* cells, but far reduced for the non-cleavable LexAK156A strain (Fig. 3d-e). Evidently, spontaneous SOS induction reflects a continuous scale of LexA degradation levels rather

than a distinct regulatory state. Because spontaneous DNA breakage is rare during normal growth (~2% of cell cycles[57]), other processes must be involved in triggering LexA degradation in a large proportion of cells. In fact, it is known that DNA replication forks frequently stall or collapse during normal growth (~once per cell cycle)[58–60]. Furthermore, *recA*- strains grow poorly even in optimal conditions and RecA filaments or foci are formed in ~13-20% of cell cycles[61,62]. It is plausible that LexA can interact with these transient RecA filaments, and that variation in their size and lifetime affects LexA cleavage rates. This, together with a basal rate of RecA-independent auto-cleavage, would lead to the high frequency and heterogeneity of LexA degradation seen in untreated cells. Despite the variability in the basal state of LexA, UV treatment caused complete and uniform degradation (Fig. 3f), showing high fidelity in DNA damage signalling.

These observations raise the question of how LexA's variability affects SOS gene repression. Single cells growing unperturbed inside microfluidic channels exhibited frequent expression pulses of the transcriptional SOS reporter PrecA-GFP (Fig. 4a, Extended Data Fig. 9a,b). Pulse amplitudes had a skewed distribution with many small spikes and a long tail of infrequent large pulses (Fig. 4b). Cells expressing the non-cleavable LexAG85D mutant did not show any pulses and had lower basal expression (Fig. 4a-c). This indicates that frequent LexA cleavage causes partial de-repression of the SOS response in the majority of cells. To understand how natural fluctuations in regulatory input levels modulate the output of the SOS response, we quantified LexA-Halo populations and PrecA-GFP fluorescence in the same cells (Fig. 4d). We found that PrecA was strongly induced in cells with increased LexA degradation (Fig. 4d-e). Furthermore, intermediate LexA abundances translated to a continuum of PrecA expression levels (Fig. 4e inset), explaining how gradual variation in the LexA pool creates a continuous scale of SOS expression pulses. The relation between PrecA expression and the abundance of free LexA was well described by a gene regulatory function with a promoter affinity of LexA between 2-10 nM[52,63] (Fig. 4e). The same function also matched PrecA-GFP expression in the Δ*dam* strain with increased LexA degradation (Fig. 4e), but the distribution of cells along the curve was altered, as expected. Expression of the constitutive PpolA promoter was independent of the state of LexA, confirming that the observed regulation is specific to SOS-controlled genes (Extended Data Fig. 10).

Many of the survival mechanisms induced by the SOS response impose a substantial fitness cost, and therefore must be repressed reliably in the absence of stress, despite the basal LexA fluctuations. SOS induction of the cell division inhibitor SulA is one such mechanism. Indeed, spontaneous SOS expression pulses were correlated with increased cell cycle duration (Extended Data Fig. 9c,d). Closer inspection of this relation showed that rare large expression pulses were associated with pronounced cell cycle delays, whereas frequent smaller pulses only had a minor effect on cell cycle duration (Extended Data Fig. 9c,d). In agreement with this, cells switched to filamentous growth when the free LexA pool declined below a threshold of P_{free}<30% (Fig. 4f). Only 5% of cells had such low LexA abundance, and any variation in the free LexA pool above the threshold did not influence cell length or the probability of filamentation (Fig. 4f). The switch-like control of filamentous growth ensures that the cell cycle and cell size homeostasis are robust to LexA variability. Interestingly, a related phenomenon is seen in the eukaryotic DNA damage response, where transient induction of the tumour suppressor p53 occurs under non-stressed conditions[64].

Similar to LexA, p53 pulses are only translated into cell cycle arrest when DNA damage signaling is sustained. These observations add to a growing appreciation that the genetic networks governing the DNA damage response share widespread similarities between bacteria and eukaryotes[65,66].

Our findings demonstrate that LexA achieves a remarkable balance as a master regulator, ensuring reliable repression and induction of the SOS response, while also generating gene expression variability that can act as a source of cellular variability to enhance stress resistance of isogenic bacterial populations. Because of the continuous scale of LexA degradation levels, spontaneous SOS induction is not restricted to a distinct subpopulation of cells per se, but costly SOS outputs such as filamentation are only expressed in a small number of cells when LexA abundances drop below a threshold. Such a mechanism also agrees with models that explain the stability of the lysogenic state of lambda prophages, whose SOS-dependent activation follows threshold behaviour[67,15]. The negative feedback autoregulation of LexA buffers variation in degradation rates to stabilise protein levels[68]. Single-molecule tracking of LexA-Halo provides a direct and quantitative readout of the SOS response, and the approach is applicable to other proteins that are cleaved in an SOS-dependent manner, such as lambda phage repressors[9,15,16] and DNA translesion polymerase UmuD[3,16]. The method is sensitive and bypasses key limitations of existing SOS reporters based on gene expression, opening avenues to understand how the SOS response enables bacterial survival in diverse environments.

Methods

Bacterial strains

All strains used in this study are shown in Supplementary Information Table 1 and were derived from *Escherichia coli* AB1157. The LexA-Halo fusion was generated by Lambda Red recombination[69]. We used plasmid pSU007 as a template to insert the HaloTag sequence[70] with a 27-amino acids linker at the C-terminus of the endogenous *lexA* gene followed by a kanamycin resistance cassette. The linker sequence SAEAAAKEAAAKEAAAKEAAAKAAAEF was designed to form an alpha-helical structure. The gene fusion was confirmed by colony PCR and in-gel fluorescence and the allele was moved into AB1157 wild-type strain by P1 phage transduction. The kanamycin resistance gene flanked by *frt* sites was removed by expressing Flp recombinase from plasmid pCP20. The temperature-sensitive pCP20 plasmid was cured by growing cells at 37°C, generating strain SU225.

Strains with chromosomal gene deletions of *clpX*, *lon*, *dam*, *sulA* from the Keio collection[71] and *lexAG85D (lexA3 Ind-)* were obtained from the Coli Genetic Stock Center. The alleles were moved into background strain SU225 using P1 phage transduction with selection for kanamycin or tetracycline resistance, as appropriate. Gene deletions were confirmed by colony PCR and the *lexAG85D* allele by UV sensitivity. To combine multiple deletions, antibiotic resistance genes flanked by frt sites were removed using pCP20 as above. The *recA*- allele (*recAT233C*) was kindly provided by David Sherratt (strain VS90), and confirmed by its UV sensitivity. The Δ*lexA* allele was kindly provided by Rahul Kohli (strain SAMP04) and moved into AB1157 Δ*sulA* strain via P1 phage transduction with

selection for chloramphenicol resistance, and confirmed by colony PCR. The *sulA* gene deletion is necessary for viability of Δ*lexA* strains.

For plasmid expression of the LexA-Halo fusion, the *lexA-halo* allele was amplified from SU225 and inserted into plasmid pBAD24 using Gibson assembly kit (NEB) and confirmed by sequencing. LexA point mutants were made using Q5 site-directed mutagenesis kit (NEB) and confirmed by sequencing. Plasmids were transformed into SU315 Δ*lexA* Δ*sulA* strain and selection of ampicillin resistance, ensuring that the plasmid-expressed LexA-Halo fusion is the only LexA species present.

pUC19 plasmids carrying LexA-regulated promoters were generated by amplifying the promoter sequences from an *E. coli* promoter library[72]. Insertions were made into the multiple cloning site on pUC19 by restriction digestion using EcoRI and XmaI cut sites. Plasmids were transformed into SU225 expressing chromosomal LexA-Halo.

The PrecA-GFPmut2 and PpolA-GFPmut2 transcriptional reporters were copied from the promoter library plasmids[72] and inserted on the chromosome between *tam* and *yneE* genes in the chromosome terminus region[73] via Lambda Red recombination and selection for kanamycin resistance. Placement of the transcriptional reporter in the chromosome terminus region ensures it is present at a single copy during most of the replication cycle, thus minimising expression fluctuations due to gene copy number variations.

Functionality of the LexA-Halo fusion

We assessed the functionality of the LexA-Halo fusion in different ways:

1. It is known that *E. coli* strains with a Δ*lexA* gene deletion are non-viable because constitutive SOS induction of *sulA* inhibits cell division. Δ*lexA* strains are viable when combined with a Δ*sulA* deletion. We constructed the endogenous LexA-Halo fusion in a wild-type strain (*sulA* $^{+}$). This strain is fully viable and we do not see abnormal filamentation which would be expected if a partial defect of LexA-Halo caused mild SOS induction.
2. The LexA-Halo fusion strain has the same death rate as the wild-type, whereas a strain expressing non-cleavable LexAG85D has a higher spontaneous death rate (Extended Data Fig. 1h).
3. The basal expression level of the PrecA-GFP reporter is the same in the wild-type and LexA-Halo strains (Extended Data Fig. 1g).
4. A *lexA* complementation assay was performed based on PrecA-GFP reporter expression (Extended Data Fig. 2a-c). A Δ*lexA* Δ*sulA* strain shows high reporter expression due to constitutive SOS response activation. Complementation of Δ*lexA* with pBAD plasmids expressing wild-type LexA or LexA-Halo both repressed the PrecA reporter to the same level.
5. UV sensitivity assays were performed for wild-type, LexA-Halo, LexAG85D, and *recA*-strains (Extended Data Fig. 1a). UV survival is partially reduced for LexA-Halo compared to the wild-type, but less so than for the SOS deficient mutants LexAG85D and *recA*-. The UV survival is in the same range as reported

in other studies for *E. coli* AB1157: 20% survival at 50 J/m^2 [74], 25% survival at 60 J/m^2 [75], 10% survival at 75 J/m^2 [76].

6. The LexA-Halo strain shows the same survival as the wild-type when treated with the DNA damaging agents methyl methanesulfontate and ciprofloxacin, whereas LexAG85D and *recA*- are highly sensitive (Extended Data Fig. 1b,c).

7. The spontaneous SOS gene expression pulses of the PrecA-GFP reporter are present in the wild-type and LexA-Halo strains (Extended Data Fig. 1d-f).

8. The degradation level of LexA-Halo is correlated with PrecA-GFP target gene expression and cell filamentation in single cells (Fig. 4).

9. The LexA-Halo fusion recapitulates key aspects of known LexA function in cells, e.g. binding to specific promoter sequences (Fig. 1e), dimerization (Fig. 2f), and DNA-damage induced cleavage (Fig. 2a).

10. Labelling LexA-Halo with TMR does not perturb function: (i) The D distribution of LexA-Halo does not depend on the concentration of TMR dye used for labelling (Extended Data Fig. 2e). (ii) The D distribution of LexA-Halo labelled with TMR before UV treatment is the same as for cells that were first exposed to UV and subsequently labelled with TMR. In both cases, LexA-Halo is fully converted into the free Halo tag (Extended Data Fig. 2f). (iii) TMR labelling does not affect cell viability or UV sensitivity (Extended Data Fig. 2g).

These characterisations establish that LexA-Halo is a functional reporter for LexA function in cells. The fact that the basal expression level of the PrecA reporter is the same in the wild-type and LexA-Halo fusion strains indicates that the fusion does not alter LexA abundance in cells. The increased sensitivity of the LexA-Halo fusion strain to a UV pulse is notable. No increase in sensitivity is seen for constant chemical DNA damage treatment (Extended Data Fig. 1). During SOS response activation, LexA cleavage is triggered by binding to the RecA filament with interaction across its N- and C-terminal domains[77]. It is likely that the increased UV sensitivity is attributable to the C-terminal HaloTag fusion causing a steric hindrance that partially hinders the interaction of LexA with RecA filaments, but does not completely prevent this interaction. The C-terminal fusion would not perturb the N-terminal DNA-binding domain of LexA and hence SOS gene repression is unaffected, as observed.

A key result in this article is that LexA is frequently degraded during normal growth, which in turn leads to SOS gene expression heterogeneity. Notably, a partial decrease in LexA cleavage due to the HaloTag means that the degradation of wild-type LexA should be even more frequent, and hence SOS gene expression variation should be more pronounced in the wild-type. This is indeed what we observe. The distribution of PrecA-GFP expression is broader and spontaneous expression pulses are elevated in the wild-type strain compared to the LexA-Halo strain (Extended Data Fig. 1g).

Cell culture and HaloTag labelling

Strains were streaked from frozen glycerol stocks on to LB agarose with appropriate antibiotic selection. A single colony was used to inoculate LB (+ appropriate antibiotic if strain carried a plasmid) and grown for 6-7 hours. The cultures were then diluted 1:1000 into

supplemented M9 minimal medium containing M9 salts (15 g/L KH2PO4, 64 g/L Na2HPO4, 2.5 g/L NaCl, 5.0 g/L NH4Cl), 2 mM MgSO4, 0.1 mM CaCl2, 0.5 μg/ml thiamine, MEM amino acids, 0.1 mg/ml L-proline, 0.2% glucose. Cultures were grown overnight to stationary phase, then diluted 1:100 into supplemented M9 medium and grown to OD600 0.1-0.2 before labelling the HaloTag. For strains expressing LexA-Halo (and LexA mutants) from pBAD plasmid, growth medium containing 0.2% glycerol instead of glucose was used to induce leaky expression. This resulted in similar LexA expression levels as in the strains with chromosomal expression.

We labelled LexA-Halo covalently with TMR dye in live cells according to the protocol described before[39]. Briefly, cell culture was concentrated 10-fold by centrifugation. 100 μl of cell suspension was incubated with 2.5 μM TMR ligand (Extended Data Fig. 2d) (Promega) at 25°C for 30 min, followed by 4 rounds of washing, centrifugation, and resuspension in 1 ml of M9 medium to remove free dye from the culture. For dual-colour imaging with PrecA-GFP, we labelled LexA-Halo with JF549[78] instead of TMR, using the same labelling protocol. The enhanced photostability of JF549 compared to TMR increases the number of tracks obtained per cell[39], which facilitated the single-cell diffusion analysis. After labelling and washing, cells were recovered for 30 min shaking at 37°C to resume growth and allow free dye to diffuse out of cells, which was removed by a further wash with 1 ml of M9 medium. This step was crucial to reduce background fluorescence contamination during single-molecule imaging[39]. After the removal of free dye, cell growth and division gradually dilutes the fluorescently-labelled LexA pool as new unlabelled proteins are synthesised.

For experiments with fixed cells, we labelled LexA-Halo with TMR as above and subsequently resuspended cells in 2.5% paraformaldehyde solution in PBS buffer. Cells were fixed for 30 min at room temperature and washed once in PBS before imaging.

Following labelling, cells were resuspended in approximately 10 μl M9 medium and spotted onto 1% low-fluorescence agarose pads (Bio-Rad) prepared in M9 medium and covered with a no1.5 glass coverslip. Coverslips were treated with air plasma (Plasma Etch) prior to use to remove fluorescent background particles. For UV treatment, cells were placed on the agarose pad and exposed to a UV pulse using a Stratalinker 1800 lamp at the indicated doses before covering with a coverslip. Slides were then incubated at 22°C and multiple fields of view were recorded per slide for up to 45 min for untreated cells, or at the indicated times post UV exposure.

Single-molecule tracking

Single-molecule imaging was performed using a custom-built total internal reflection fluorescence (TIRF) microscope[38] under oblique illumination at 22°C. Movies and snapshots were acquired using Andor Solis software. Initially, cells in a field of view were exposed to 561 nm laser illumination at 0.5 kW cm^{-2} for around 30 seconds such that there was less than one molecule in the fluorescent state per cell on average. We recorded movies of 10-20 thousand frames under continuous 561 nm excitation at 0.5 kW cm^{-2} at a rate of 7.48 ms/frame. TMR and JF549 dyes switch reversibly between dark and bright states. The dark state is long-lived such that the majority of molecules are off at any time and only a

small subset stochastically switches to the bright state. The bright state is sufficiently stable to track a single molecule for several frames until deactivation or photobleaching. This allows measuring tens to hundreds of tracks per cell[39] (Extended Data Fig. 8a). A transmitted light image generated by LED illumination was recorded for each field of view for the purpose of cell segmentation.

For dual-colour LexA-Halo and PrecA-GFPmut2 or PpolA-GFPmut2 imaging, we first recorded a 100-ms snapshot with 488 nm illumination at 0.1 kW cm^{-2}, followed by a movie of LexA-Halo-JF549 under 561 nm illumination at 0.5 kW cm^{-2} of the same cells.

Custom-written MATLAB software (Mathworks) was used for localisation[79], tracking[80] and calculation of diffusion coefficients[81]. Cell outlines were automatically segmented from transmitted light images using a modified version of MicrobeTracker[82] combined with SuperSegger[83]. Apparent diffusion coefficients (D) were calculated from the Mean Squared Displacement (MSD) averaged over 4 steps per molecule: $D = MSD/(4 \cdot \Delta t)$, with $\Delta t = 7.48$ ms. Shorter tracks were discarded and longer tracks were truncated to 4 steps. The number of tracks reported in the figure legends refer to tracks with 4 or more steps. Distributions of diffusion coefficients represent the accumulated tracks from biologically independent repeats with a total number of cells as indicated in the figure legends (as in Fig. 1 & 2) or of single cells (as in Fig. 3). The number of repeats reported throughout refers to biologically independent experiments from separate cell cultures and performed on different days. Pearsson's correlation coefficients were computed using the corrcoef function in MATLAB with default parameters.

Because TMR and JF549 fluorophores switch repeatedly between dark and bright states, individual molecules can be observed multiple times over the course of a movie. Furthermore, although we have optimised our labelling procedure to saturate HaloTag labelling (Extended Data Fig. 2d), the labelling efficiency is unknown. Therefore, the absolute number of tracks is not a direct measure of the number of LexA molecules. Here, we quantified the relative abundances of LexA populations based on the number of tracks in a particular diffusion state normalized by the total track counts per cell. In our previous work (e.g.[84]) we used analytical distributions that described diffusion characteristics of a single protein species that exists in multiple diffusive states (e.g. DNA-bound, transiently DNA-interacting, freely diffusing). However, for LexA we found this approach was not appropriate. This was because a variety of different LexA species are present in the cell (e.g. various types of cleavage and degradation intermediates and monomer/dimer states). Instead, we fitted D distributions with model curves using linear regression. We used calibration measurements to generate empirical D distributions for the bound (D_{bound}), free (D_{free}), and degraded ($D_{degraded}$) LexA species. The model curve for the bound population was obtained from measuring LexA-Halo in cells fixed with paraformaldehyde. The model curve for the free LexA pool was obtained from cells expressing the non-cleavable LexA K156A mutant. The model curve for the degraded population was obtained from cells expressing unconjugated HaloTag. Model curves were smoothed using moving mean filters. Measured D distributions ($D_{measured}$) were then fitted with these empirical model curves by linear least-squares regression using MATLAB lsqlin. The function minimises $(NORM(D_{model} * P - D_{measured}))^2$. where $D_{measured}$ is a vector of the histogram bins, $D_{model} = [D_{bound}, D_{free},$

$D_{degraded}$] is a matrix of size 3 x histogram bins, and $P = [P_{bound}, P_{free}, P_{degraded}]$. The resulting coefficients P give the LexA population abundances, constrained such that $P_{bound} + P_{free} + P_{degraded} = 1$. Each fit was averaged over 100 bootstrapping repeats. Fitting results are summarized in Supplementary Information Table 2.

The unconjugated HaloTag distribution shows an immobile population of $P_{bound} = 1.3\pm0.4\%$, which represents residual TMR dye that remains after the labelling and washing procedure and also reflects a low level of non-specifically bound HaloTag[39]. This background level matches the residual bound population of LexA-Halo after complete degradation post 50 J/m^2 UV treatment. Therefore, in order to compare the bound LexA population to the number of LexA-regulated promoters, we deducted this background level from the P_{bound} estimate for LexA in the wild-type strain, giving an estimate of $P_{bound} = 4.8\pm0.4\%$. Note that because the number of tracks differs between cells, the mean population abundances from the accumulated D distribution of multiple cells are not the same as the mean of the population abundances from multiple single-cell D distributions. For example, for endogenous LexA-Halo in untreated cells, $P_{degraded} = 32.0\%$ for the accumulated tracks, and $P_{degraded} = 22.1\%$ for the mean of the single-cell abundances. For single-cell analysis of LexA populations, cells with less than 25 tracks (with >4 localizations) were excluded to ensure reliable distribution fitting (~10% of cells).

For dual-colour measurements, the PrecA-GFPmut2 or PpolA-GFPmut2 intensity per cell was measured from the average pixel intensity within each segmented cell area and the median background intensity outside cells was subtracted.

In-gel Halo-TMR fluorescence

Cells expressing HaloTag fusions were grown and labelled with TMR dye as for single-molecule imaging, but washed only once with 1 ml M9 medium. Cells were pelleted after labelling and lysed in 30 µl SDS sample buffer heated at 95°C for 5 min. Halo-tagged species were separated via SDS-PAGE and imaged on a gel scanner with 532 nm laser excitation (Fujifilm Typhoon FLA 7000). Band intensities were quantified using ImageJ and the relative abundance of the degraded LexA population was calculated from the ratio HaloTag/(LexA-Halo + HaloTag).

Single-cell microfluidics

Mothermachine microfluidic experiments were performed as described[4] to measure PrecA-GFPmut2 expression dynamics during continuous unperturbed growth in M9 glucose medium at a single-cell level. Cells expressed fluorescent protein mKate2 constitutively and carried an *flhD* gene deletion to remove flagellum motility. Imaging was performed on a Nikon Ti Eclipse inverted fluorescence microscope equipped with perfect focus system, 100x NA1.45 oil immersion objective, sCMOS camera (Hamamatsu Flash 4), motorized stage, and 37°C temperature chamber (Okolabs). Fluorescence images were automatically collected using NIS-Elements software (Nikon) and an LED excitation source (Lumencor SpectraX). Time-lapse movies were recorded at 3-min intervals with 100 ms exposures for GFPmut2 and mKate2 using 50% LED excitation intensities. Movies were analysed using custom Matlab software to segment cells based on cytoplasmic mKate2 fluorescence and to

construct single-cell lineages. PrecA-GFPmut2 expression traces represent the average pixel intensity within the area of a cell in each frame after subtracting the median background signal outside cells. Expression pulses were identified by applying a moving mean filter (30 frames window) and using *findpeaks* function in Matlab.

Extended Data

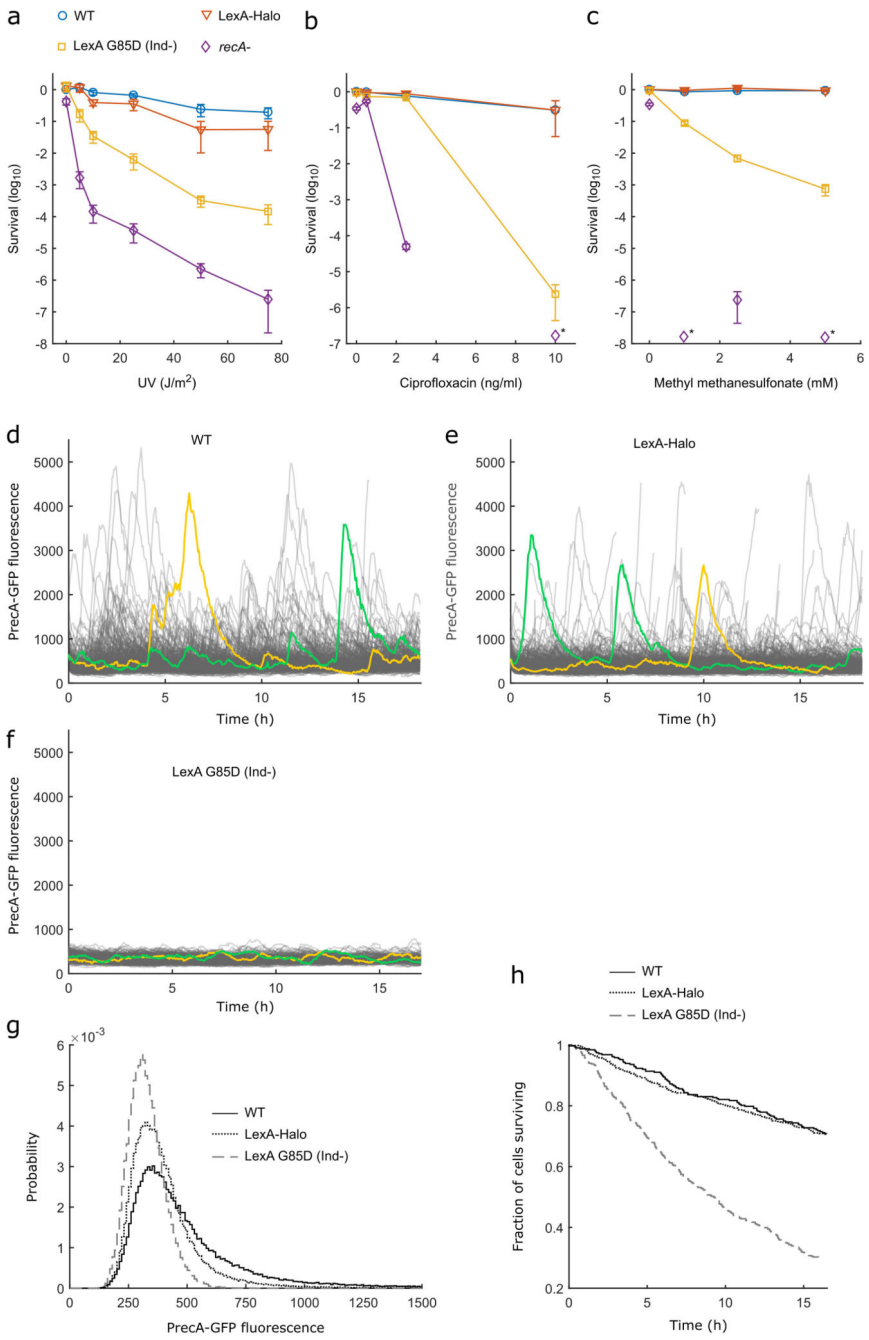

Extended Data Fig. 1. Assessing the functionality of the LexA-Halo fusion.

Europe PMC Funders Author Manuscripts

Europe PMC Funders Author Manuscripts

a, b, c DNA damage sensitivity assays: 10-fold serial dilutions of LB cultures at OD 0.4 were spotted on LB agarose plates and exposed to indicated UV doses (a), or spotted on LB plates containing ciprofloxacin (b), or methyl methanesulfonate (c). Plates were incubated overnight. Control plates were incubated without DNA damage treatment. The percentages of surviving cells are the number of colonies on treatment plates normalised relative to the number of colonies counted for wild-type (WT) without treatment. Data are mean ±SEM from 6 repeats (UV) or 3 repeats (ciprofloxacin, MMS). * indicates zero survival observed. The LexA-Halo fusion strain shows a moderate increase in UV sensitivity compared to the wild-type AB1157 strain, while the SOS deficient strains with non-cleavable LexAG85D mutant or *recA*- mutation are hypersensitive to UV damage. LexA-Halo shows the same sensitivity to ciprofloxacin and methyl methanesulfonate as the wild-type. **d, e, f,** Functionality of LexA-Halo fusion assessed in continuous growth conditions: Single-cell fluorescence dynamics of SOS expression reporter PrecA-GFP during unperturbed growth in mothermachine microfluidic chips for cells expressing wild-type LexA (d, 310 cells), LexA-Halo (e, 501 cells), and non-cleavable LexAG85D (f, 446 cells). Two example cell traces are highlighted per strain. The LexA-Halo fusion strains shows SOS expression pulses similar to the wild-type strain. No pulses are seen in the LexA G85D strain. **g,** Distributions of PrecA-GFP fluorescence for wild-type LexA, LexA-Halo, and LexAG85D strains show that the LexA-Halo fusion is functional in SOS gene repression. The tail in the distribution for LexA-Halo shows functional SOS induction similar to the wild-type strain. The amplitudes of the SOS expression pulses were slightly reduced compared to the wild-type, matching the reduction in UV tolerance (panel A). **h,** Distributions of cell survival times during growth in microfluidic chips for wild-type LexA, LexA-Halo, and LexAG85D strains confirms functionality of the LexA-Halo fusion.

Europe PMC Funders Author Manuscripts

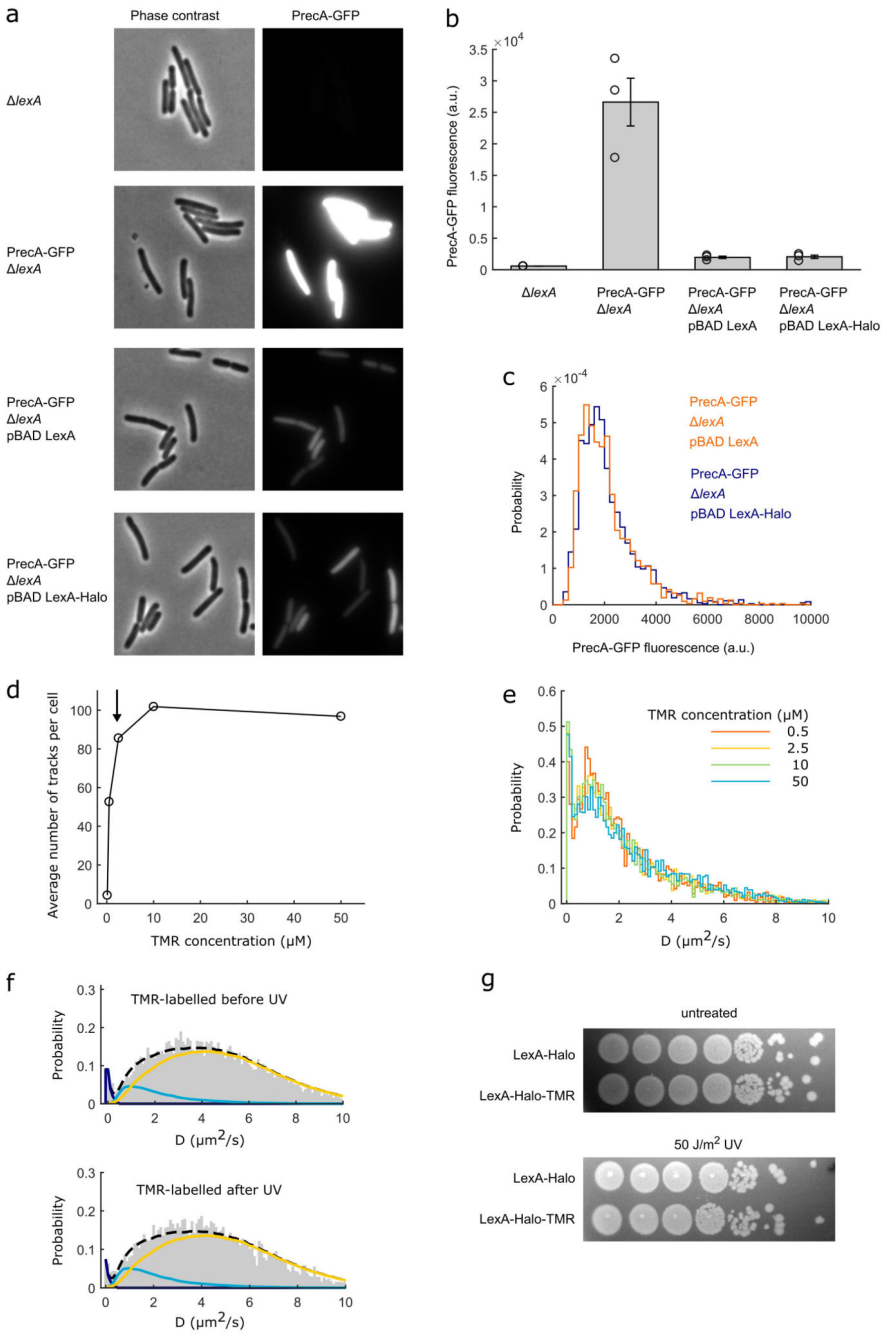

Extended Data Fig. 2. LexA-Halo complementation and characterization of HaloTag labelling.

a, Testing LexA-Halo functionality by complementation of Δ*lexA* mutant. Representative phase contrast and fluorescence snapshots from 3 independent biological repeats. The PrecA-GFP reporter shows high fluorescence in a Δ*lexA* strain because the SOS response is unrepressed. The PrecA-GFP reporter becomes repressed to the same level when the Δ*lexA* allele is complemented with pBAD plasmids expressing LexA (untagged wild-type gene) or the LexA-Halo fusion construct. The Δ*lexA* strain without PrecA-GFP reporter is included to show the level of cellular autofluorescence. **b,** Average PrecA-GFP fluorescence per cell

± SEM and individual measurements from 3 repeats. Δ*lexA*: 1195 cells; Δ*lexA* PrecA-GFP: 1268 cells; Δ*lexA* PrecA-GFP pBAD LexA: 1100 cells; Δ*lexA* PrecA-GFP pBAD LexA-Halo 1241 cells). **c,** Histograms of PrecA-GFP fluorescence for pBAD LexA (1100 cells) and pBAD-LexA-Halo (1241 cells) complementation. **d,** Characterisation of LexA-Halo labelling: Average number of observed LexA-Halo tracks per cell after labelling with different concentrations of TMR dye. The labelling efficiency saturates for TMR concentration > 2.5 μM. Arrow indicates concentration used throughout this study. **e,** D distributions for LexA-Halo do not depend on the concentration of TMR dye used for labelling. **f,** LexA degradation is unaffected by TMR labelling. D distributions for LexA-Halo 90 min after 50 J/m^2 UV treatment for cells labelled with TMR before treatment (top) and for cells labelled with TMR after UV treatment. **g,** TMR labelling does not affect cell viability or UV sensitivity. Cells expressing LexA-Halo were prepared and labelled with 2.5 μM TMR using the same protocol as for imaging, or mock-labelled in buffer only. 10-fold serial dilutions were spotted on LB agarose plates and exposed to 50 J/m^2 UV light before incubating overnight, or incubated without UV exposure.

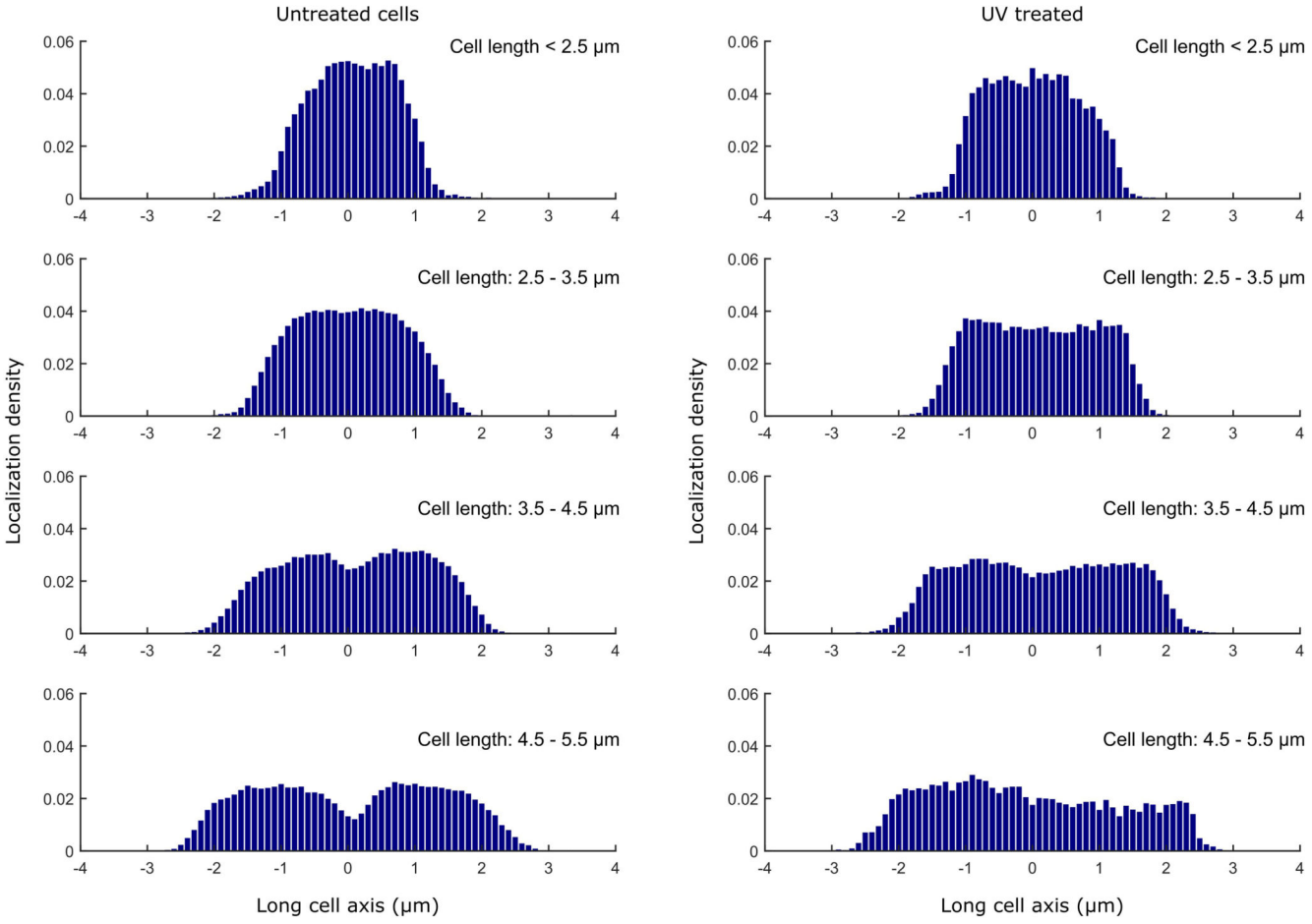

Extended Data Fig. 3. Spatial distribution of LexA.

Histograms show the density of LexA-Halo localizations projected onto the long cell axis. Cells were split into 4 classes based on length, < 2.5 μm, 2.5 – 3.5 μm, 3.5 – 4.5 μm, 4.5 –

Europe PMC Funders Author Manuscripts

5.5 μm. In untreated cells, LexA localizations reflect the typical spatial distribution of the nucleoid that splits into two lobes as cells elongate. This spatial pattern is largely absent in cells 180 min after treatment with 50 J/m^2 UV when LexA-Halo has been largely converted into free HaloTag. Untreated cells: 4 repeats, 466 cells, 500284 localizations; UV-treated cells: 3 repeats, 164 cells, 103475 localizations.

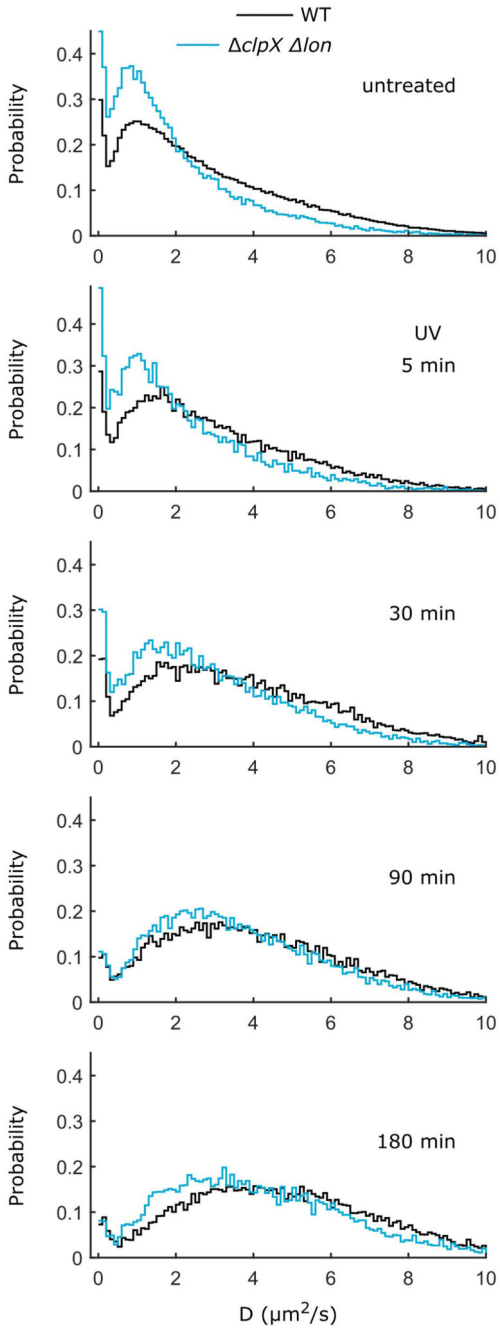

Extended Data Fig. 4. Comparison of LexA diffusion in Δ*clpX* Δ*lon* and wild-type strains without treatment and after exposing cells to a pulse of 50 J/m^2 UV.

Combined data from N = 3 repeats per time point. Untreated WT: N = 9 repeats, 2528 cells, 384241 tracks. Untreated Δ*clpX* Δ*lon*: 458 cells, 33239 tracks. 5 min WT: 280 cells, 23452 tracks. 5 min Δ*clpX* Δ*lon*: 238 cells, 11249 tracks. 30 min WT: 295 cells, 15408 tracks. 30 min Δ*clpX* Δ*lon*: 258 cells, 17578 tracks. 90 min WT: 333 cells, 18338 tracks. 90 min Δ*clpX* Δ*lon*: 232 cells, 17995 tracks. 180 min WT: 307 cells, 18391 tracks. 180 min Δ*clpX* Δ*lon*: 250 cells, 10858 tracks.

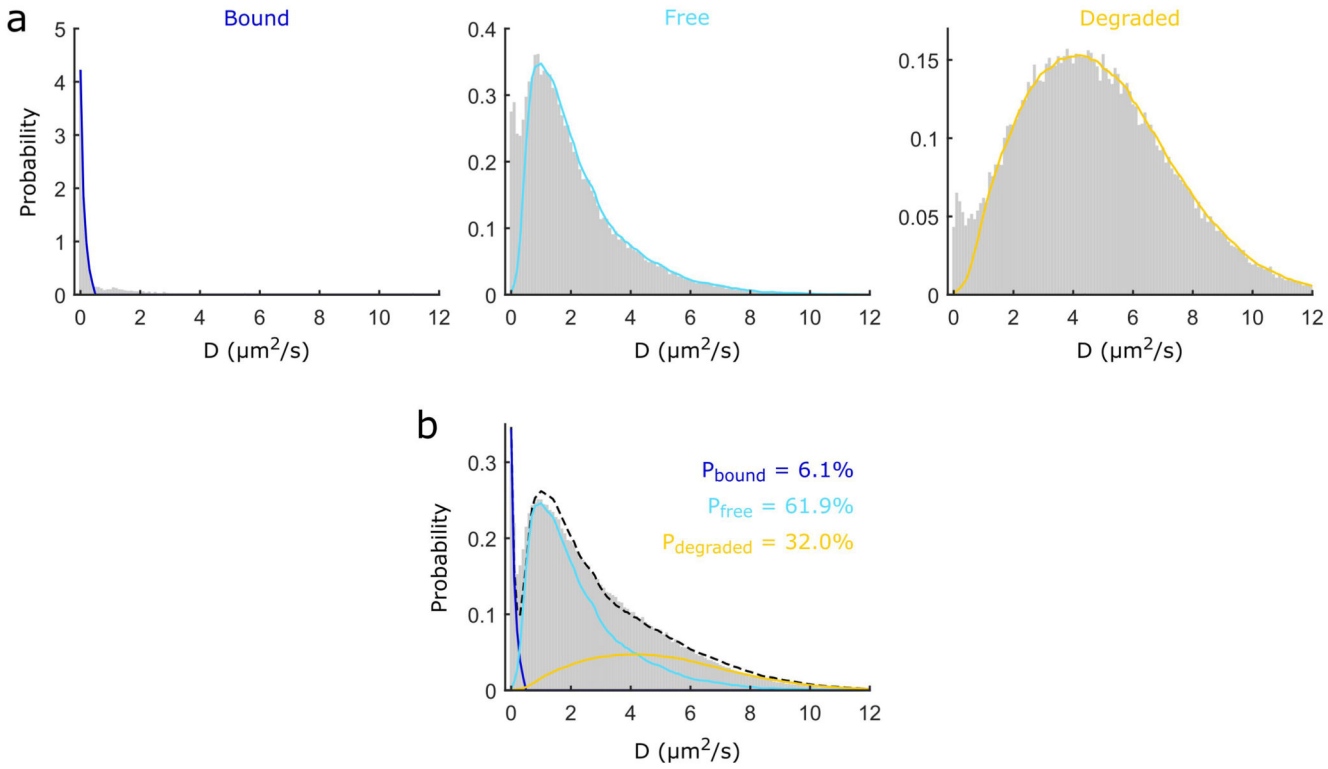

Extended Data Fig. 5. Quantifying relative abundances of LexA populations.

a, Bound, free, and degraded LexA populations were quantified by fitting a mixture model to D distributions using least squares optimization (3 repeats for each condition), as described in the Materials and Methods. The D distribution of LexA-Halo from fixed cells was used as a model for the bound population (dark blue curve). The mobile part of the D distribution for the non-cleavable LexAK156A mutant was used as a model for the free population (light blue curve). The mobile part of the D distribution for the unconjugated HaloTag was used to model the degraded population (yellow curve). The model distributions were smoothed using moving mean filters. **b,** Fitted mixture model for LexA-Halo in untreated wild-type cells.

Europe PMC Funders Author Manuscripts

Europe PMC Funders Author Manuscripts

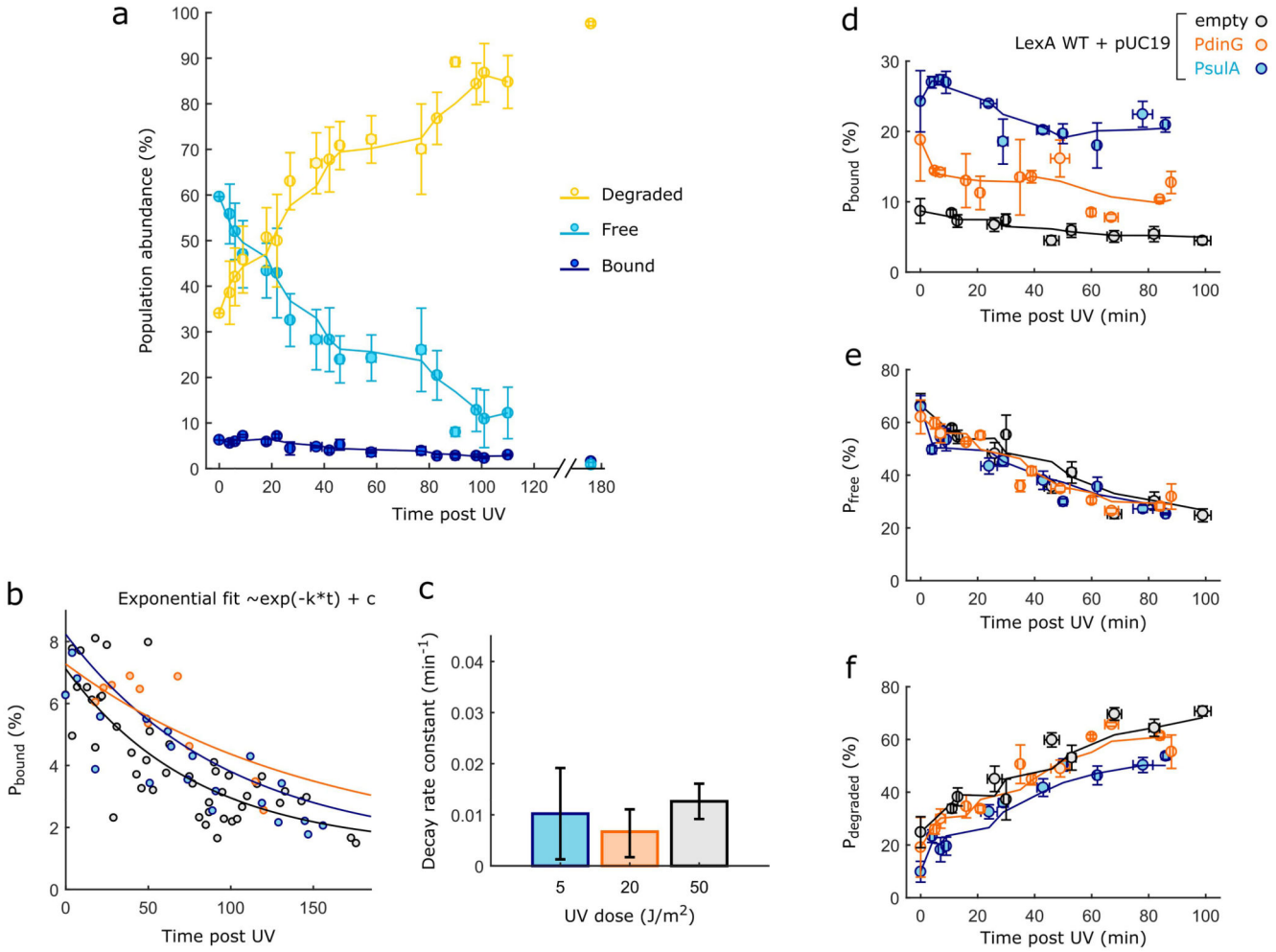

Extended Data Fig. 6. Dynamics of LexA populations after UV exposure

a, Relative abundances of degraded (yellow), free (light blue), and DNA-bound (dark blue) LexA populations after exposing cells to a pulse of 50 J/m^2 UV. LexA populations were quantified by fitting a mixture model to D distributions at different time points post UV using least squares optimization as shown in Extended Data Fig. 7 (error bars: SEM, 3 repeats, average numbers per time point: 304 cells, 15365 tracks). Lines show moving mean curves. **b,** Decay of bound LexA population post UV exposure of 5 J/m^2 (blue), 20 J/m^2 (orange), or 50 J/m^2 (grey), 1 repeat per condition. **c,** Decay rate constants were obtained from exponential fits of the data in panel b. Error bars: ± 95% confidence intervals. The decay of the bound LexA population is slower than that of the free LexA population (Fig. 2e), and the rate does not scale with UV dose. **d, e, f** Dynamics of LexA populations post 50 J/m^2 UV exposure for cells carrying empty pUC19 plasmid, pUC19 with PdinG or PsulA (error bars: SEM, N = 3 biologically independent experiments. Average numbers per time point pUC19 empty: 232 cells, 5669 tracks; PdinG: 273 cells, 13186 tracks; PsulA: 290 cells, 18724 tracks). Bound population (d), free population (e), degraded population (f).

Europe PMC Funders Author Manuscripts

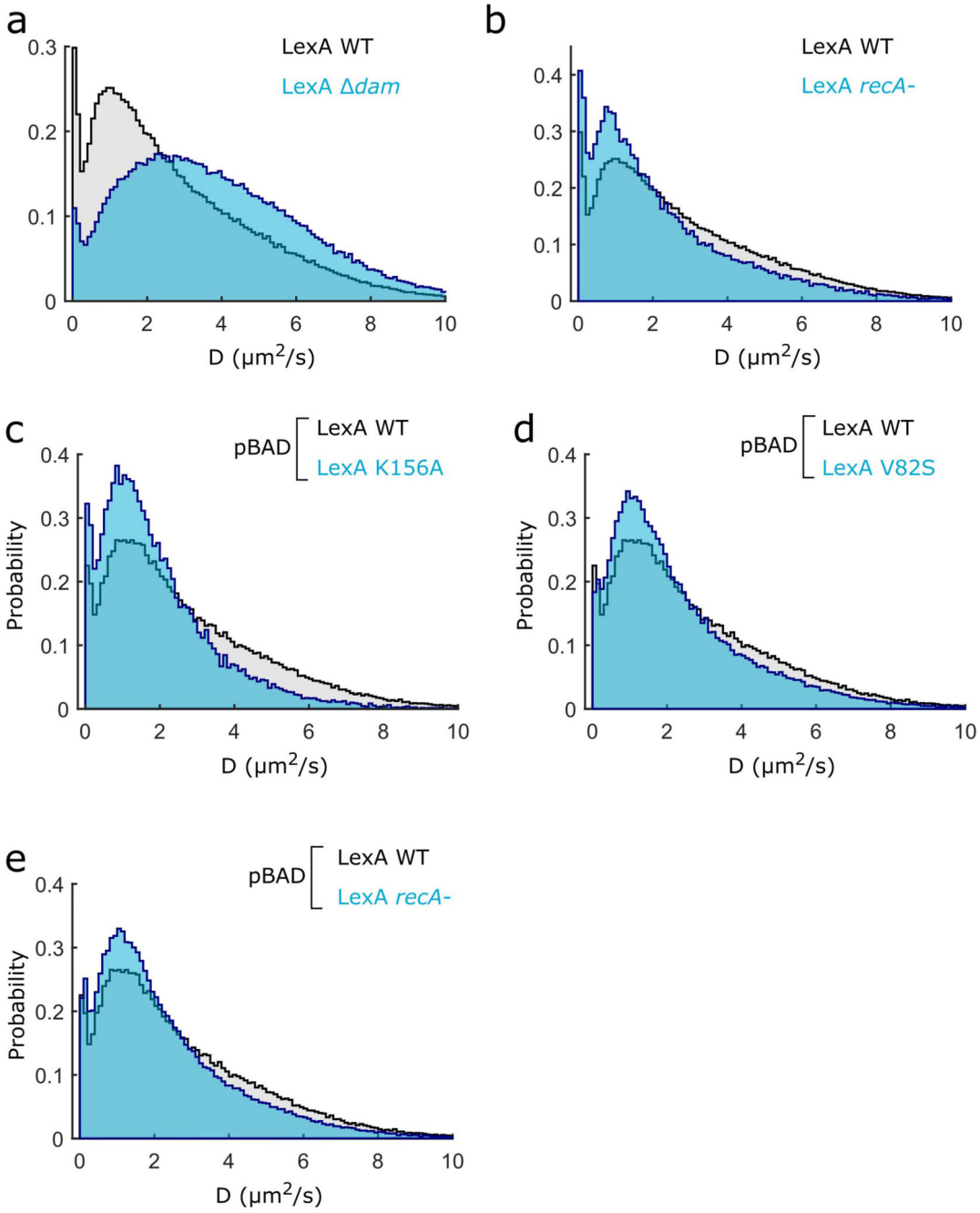

Extended Data Fig. 7. D distributions for mutant strains and LexA variants.

a, LexA-Halo in wild-type (grey, 9 repeats, 2528 cells, 384241 tracks) and Δ*dam* (blue, 3 repeats, 911 cells, 186197 tracks) strain backgrounds. **b,** LexA-Halo in wild-type (grey, 9 repeats, 2528 cells, 384241 tracks) and recA- (blue, 3 repeats, 854 cells, 41528 tracks) strain backgrounds. **c,** Wild-type LexA-Halo (grey, 5 repeats, 1265 cells, 99306 tracks) and non-cleavable LexAK156A mutant (blue, 3 repeats, 368 cells, 24343 tracks), both expressed from pBAD plasmid. **d,** Wild-type LexA-Halo (grey, 5 repeats, 1265 cells, 99306 tracks) and auto-cleavage deficient LexAV82S mutant (blue, 3 repeats, 1096 cells, 116653 tracks), both

expressed from pBAD plasmid. **e,** Wild-type LexA-Halo (grey, 5 repeats, 1265 cells, 99306 tracks) expressed from pBAD plasmid in wild-type (grey) and recA- (blue, 934 cells, 3 repeats, 1511 cells, 153981 tracks) strain backgrounds.

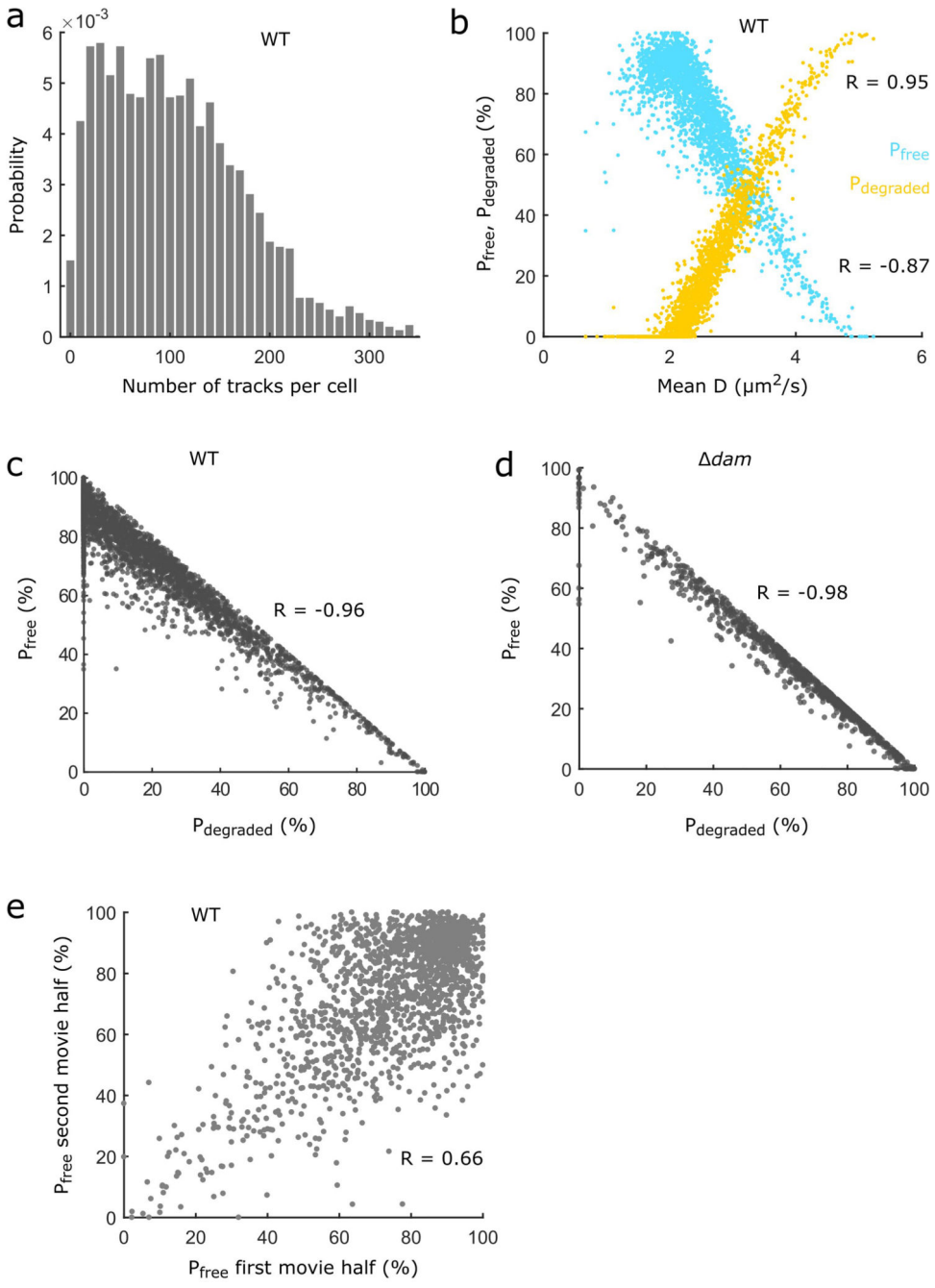

Extended Data Fig. 8. Quantification of LexA populations in single cells.

a, Distribution of the number of tracks per cell for LexA-Halo wild-type. **b,** The abundances of P_{free} and $P_{degraded}$ are highly correlated with the average diffusion coefficient of LexA-Halo per cell. Each dot represents a single cell from the wild-type LexA-Halo strain. R:

Pearsson's correlation coefficient. **c, d,** Plots of P_{free} versus $P_{degraded}$ show that increased level of LexA degradation is correlated with a loss of the pool of free LexA in individual cells from the wild-type and the Δ*dam* strain background. R: Pearsson's correlation coefficient. **e,** Evaluation of the statistical fitting error for single cells: Recorded movies were split into two halves, and single-cell quantification of LexA populations was performed independently for each movie half. P_{free} from the two movie segments are correlated (R: Pearsson's correlation coefficient) with a mean absolute difference of 16%, showing that the cell-to-cell variation in LexA abundances is not due to fitting uncertainty. Note that the actual fitting uncertainty is yet lower because the analysis includes the full-length movie data.

Europe PMC Funders Author Manuscripts

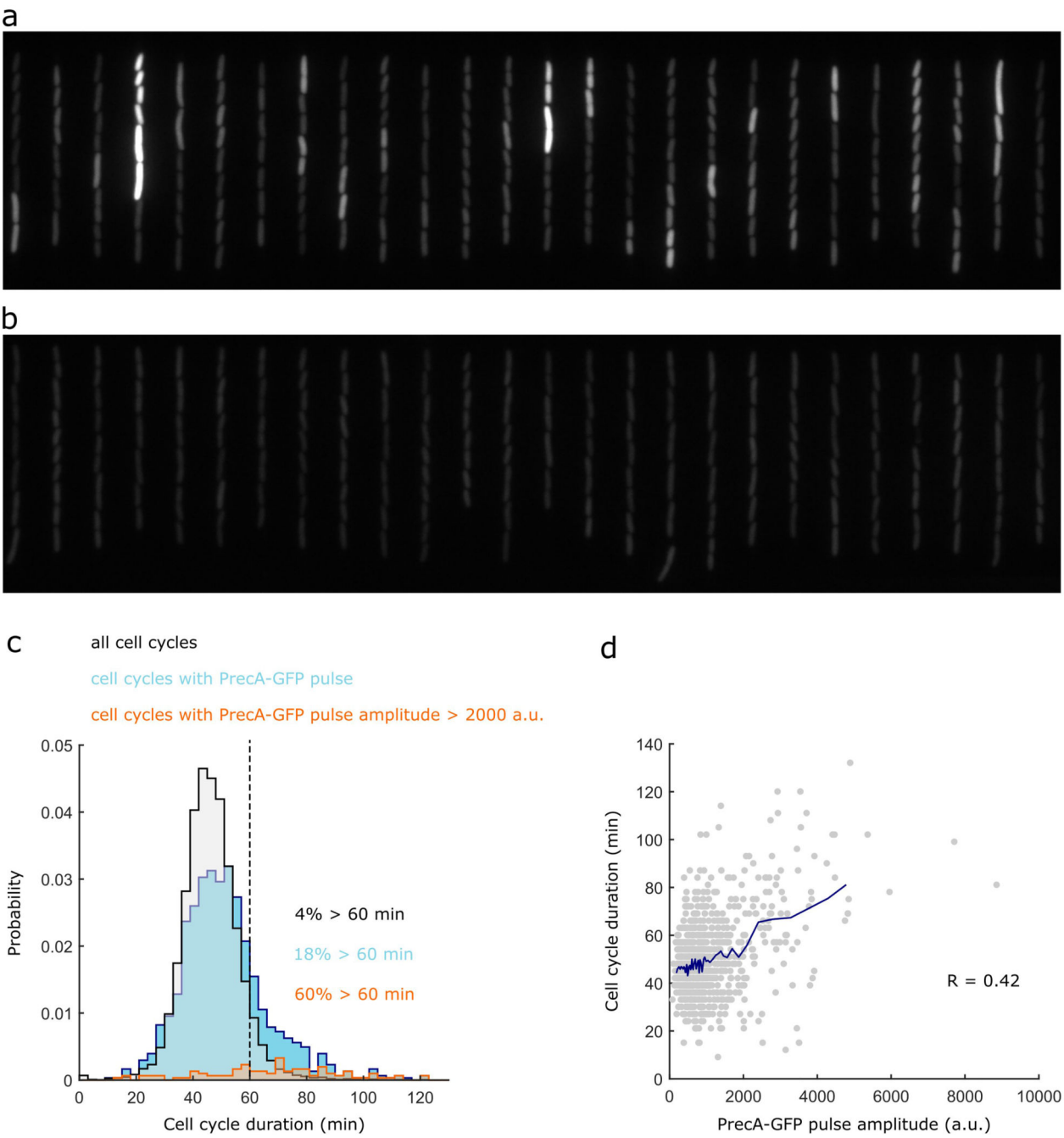

Extended Data Fig. 9. Spontaneous SOS expression pulses are associated with a cell cycle delay.

a, Snapshots of PrecA-GFP expression reporter for untreated cells growing in microfluidic channels. Continuous scale of spontaneous SOS induction levels in wild-type cells. **b,** No SOS expression pulses are seen in the LexAG85D mutant strain. Identical greyscale as in panel a. **c,** Histogram of cell cycle durations for wild-type cells growing in microfluidic channels. All cell cycles (grey, 16076 cycles), cell cycles that contain a PrecA-GFP expression pulse (blue, 1013 cycles), cell cycles that contain a PrecA-GFP expression pulse with amplitude > 2000 a.u. (orange, 102 cycles). Percentage of cell cycles with duration >

60 min shown for each category (dashed line). 3 repeats. **d,** PrecA-GFP pulse amplitude plotted versus the duration of the cell cycle that contained the pulse (3 repeats, 1013 pulses). Pulse amplitude and cell cycle duration are correlated, R: Pearsson's correlation coefficient. Moving average curve (blue line) shows a minor cell cycle delay for small PrecA-GFP pulses, but a strong delay for pulses with amplitude > 2000 a.u.

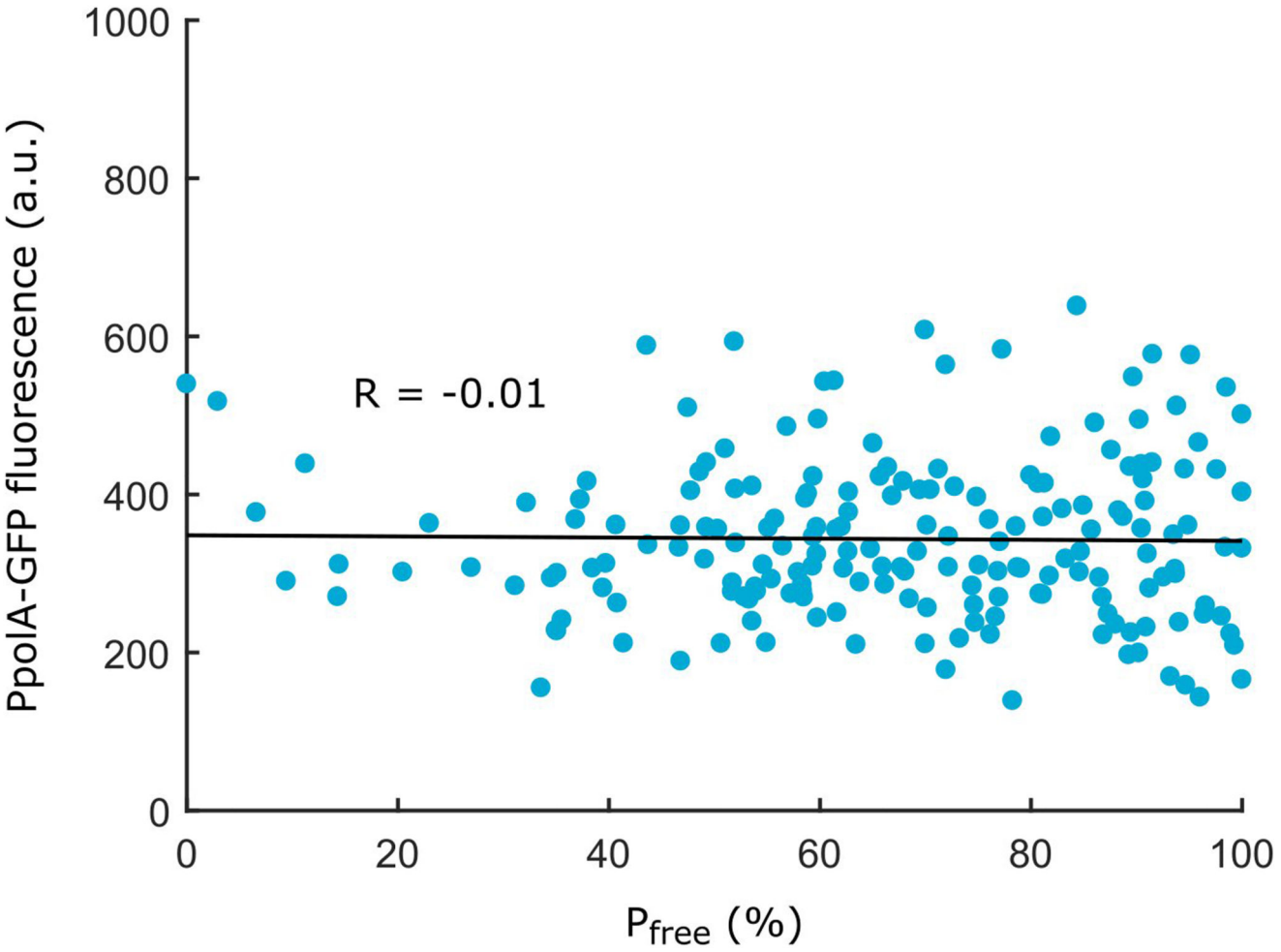

Extended Data Fig. 10. No correlation between LexA variability and expression of a gene that is not part of the SOS regulon.

Imaging PpolA-GFP expression and tracking LexA-Halo diffusion in the same cells shows that there is no correlation between gene expression and the free LexA abundance per cell. Each dot represents a single cell. Black line shows linear fit; R: Pearsson's correlation coefficient.

Supplementary Material

Refer to Web version on PubMed Central for supplementary material.

Acknowledgments

We thank Rahul Kohli (University of Pennsylvania) and David J. Sherratt (University of Oxford) for providing strains, and members of the Uphoff group and David Sherratt's group for discussions. We thank Aditya Jalin for his contributions during a lab internship. Funding: Research in the Uphoff lab is funded by a Wellcome Trust & Royal Society Sir Henry Dale Fellowship (206159/Z/17/Z to SU), a Wellcome-Beit Prize (206159/Z/17/B to SU), and a Research Prize Fellowship of the Lister Institute of Preventative Medicine (SU). ECJ was supported by a Crankstart scholarship. SU holds a Hugh Price Fellowship at Jesus College, Oxford. The funders had no role in study design, data collection and analysis, decision to publish or preparation of the manuscript.

Data availability

Numerical data and full-length gel scans are provided as source data files with this paper. The tracking data associated with this article have been deposited at Oxford University Research Archive (ORA): https://ora.ox.ac.uk/objects/uuid:84d35d02-acb0-4d1c-af30-8045afd32542.

Code availability

MATLAB script for LexA diffusion analysis of the tracking data is available at Oxford University Research Archive (ORA): https://ora.ox.ac.uk/objects/uuid:84d35d02-acb0-4d1c-af30-8045afd32542. Other code available upon request.

References

1. Baharoglu Z, Mazel D. SOS, the formidable strategy of bacteria against aggressions. FEMS Microbiol Rev. 2014; 38:1126–1145. [PubMed: 24923554]
2. Courcelle J, Khodursky A, Peter B, Brown PO, Hanawalt PC. Comparative gene expression profiles following UV exposure in wild-type and SOS-deficient Escherichia coli. Genetics. 2001; 158:41–64. [PubMed: 11333217]
3. Schlacher K, Goodman MF. Lessons from 50 years of SOS DNA-damage-induced mutagenesis. Nat Rev Mol Cell Biol. 2007; 8:587–594. [PubMed: 17551516]
4. Uphoff S. Real-time dynamics of mutagenesis reveal the chronology of DNA repair and damage tolerance responses in single cells. Proc Natl Acad Sci. 2018; 115:E6516–E6525. [PubMed: 29941584]
5. Beaber JW, Hochhut B, Waldor MK. SOS response promotes horizontal dissemination of antibiotic resistance genes. Nature. 2004; 427:72–74. [PubMed: 14688795]
6. Ubeda C, et al. Antibiotic-induced SOS response promotes horizontal dissemination of pathogenicity island-encoded virulence factors in staphylococci. Mol Microbiol. 2005; 56:836–844. [PubMed: 15819636]
7. Guerin É, et al. The SOS Response Controls Integron Recombination. Science. 2009; 324:1034–1034. [PubMed: 19460999]
8. Kimmitt PT, Harwood CR, Barer MR. Toxin gene expression by shiga toxin-producing Escherichia coli: the role of antibiotics and the bacterial SOS response. Emerg Infect Dis. 2000; 6:458–465. [PubMed: 10998375]
9. Livny J, Friedman DI. Characterizing spontaneous induction of Stx encoding phages using a selectable reporter system. Mol Microbiol. 2004; 51:1691–1704. [PubMed: 15009895]
10. Mrak P, Podlesek Z, van Putten JPM, Zgur-Bertok D. Heterogeneity in expression of the Escherichia coli colicin K activity gene cka is controlled by the SOS system and stochastic factors. Mol Genet Genomics MGG. 2007; 277:391–401. [PubMed: 17216493]
11. Turnbull L, et al. Explosive cell lysis as a mechanism for the biogenesis of bacterial membrane vesicles and biofilms. Nat Commun. 2016; 7 11220 [PubMed: 27075392]

12. Mavridou DAI, Gonzalez D, Kim W, West SA, Foster KR. Bacteria Use Collective Behavior to Generate Diverse Combat Strategies. Curr Biol. 2018; 28:345–355. e4 [PubMed: 29395918]
13. Vogel J, Argaman L, Wagner EGH, Altuvia S. The small RNA IstR inhibits synthesis of an SOS-induced toxic peptide. Curr Biol CB. 2004; 14:2271–2276. [PubMed: 15620655]
14. Kelley WL. Lex marks the spot: the virulent side of SOS and a closer look at the LexA regulon. Mol Microbiol. 2006; 62:1228–1238. [PubMed: 17042786]
15. Zong C, So L, Sepúlveda LA, Skinner SO, Golding I. Lysogen stability is determined by the frequency of activity bursts from the fate-determining gene. Mol Syst Biol. 2010; 6:440. [PubMed: 21119634]
16. Helfrich S, et al. Live cell imaging of SOS and prophage dynamics in isogenic bacterial populations. Mol Microbiol. 2015; 98:636–650. [PubMed: 26235130]
17. Nanda AM, Thormann K, Frunzke J. Impact of Spontaneous Prophage Induction on the Fitness of Bacterial Populations and Host-Microbe Interactions. J Bacteriol. 2015; 197:410–419. [PubMed: 25404701]
18. Dörr T, Lewis K, Vulić M. SOS response induces persistence to fluoroquinolones in Escherichia coli. PLOS Genet. 2009; 5 e1000760 [PubMed: 20011100]
19. Mok WWK, Brynildsen MP. Timing of DNA damage responses impacts persistence to fluoroquinolones. Proc Natl Acad Sci. 2018; 201804218 doi: 10.1073/pnas.1804218115
20. Peyrusson F, et al. Intracellular Staphylococcus aureus persisters upon antibiotic exposure. Nat Commun. 2020; 11:1–14. [PubMed: 31911652]
21. McCool JD, et al. Measurement of SOS expression in individual Escherichia coli K-12 cells using fluorescence microscopy. Mol Microbiol. 2004; 53:1343–1357. [PubMed: 15387814]
22. Kamenšek S, Podlesek Z, Gillor O, Zgur-Bertok D. Genes regulated by the Escherichia coli SOS repressor LexA exhibit heterogeneous expression. BMC Microbiol. 2010; 10:283. [PubMed: 21070632]
23. Friedman N, Vardi S, Ronen M, Alon U, Stavans J. Precise temporal modulation in the response of the SOS DNA repair network in individual bacteria. PLoS Biol. 2005; 3
24. Manina G, Griego A, Singh LK, McKinney JD, Dhar N. Preexisting variation in DNA damage response predicts the fate of single mycobacteria under stress. EMBO J. 2019; 0 e101876
25. Pennington JM, Rosenberg SM. Spontaneous DNA breakage in single living Escherichia coli cells. Nat Genet. 2007; 39:797–802. [PubMed: 17529976]
26. Veening J-W, Smits WK, Kuipers OP. Bistability, epigenetics, and bet-hedging in bacteria. Annu Rev Microbiol. 2008; 62:193–210. [PubMed: 18537474]
27. Balázsi G, van Oudenaarden A, Collins JJ. Cellular decision making and biological noise: from microbes to mammals. Cell. 2011; 144:910–925. [PubMed: 21414483]
28. Vincent MS, Uphoff S. Bacterial phenotypic heterogeneity in DNA repair and mutagenesis. Biochem Soc Trans. 2020; 48:451–462. [PubMed: 32196548]
29. Lestas I, Vinnicombe G, Paulsson J. Fundamental limits on the suppression of molecular fluctuations. Nature. 2010; 467:174–178. [PubMed: 20829788]
30. Da Re S, et al. The SOS response promotes qnrB quinolone-resistance determinant expression. EMBO Rep. 2009; 10:929–933. [PubMed: 19556999]
31. Pribis JP, et al. Gamblers: An Antibiotic-Induced Evolvable Cell Subpopulation Differentiated by Reactive-Oxygen-Induced General Stress Response. Mol Cell. 2019; 74:785–800. e7 [PubMed: 30948267]
32. Matic I. Mutation Rate Heterogeneity Increases Odds of Survival in Unpredictable Environments. Mol Cell. 2019; 75:421–425. [PubMed: 31398322]
33. Łoś JM, Łoś M, Węgrzyn A, Węgrzyn G. Altruism of Shiga toxin-producing Escherichia coli: recent hypothesis versus experimental results. Front Cell Infect Microbiol. 2013; 2
34. Hilfinger A, Paulsson J. Separating intrinsic from extrinsic fluctuations in dynamic biological systems. Proc Natl Acad Sci U S A. 2011; 108:12167–12172. [PubMed: 21730172]
35. Durfee T, Hansen A-M, Zhi H, Blattner FR, Jin DJ. Transcription Profiling of the Stringent Response in Escherichia coli. J Bacteriol. 2008; 190:1084–1096. [PubMed: 18039766]

36. Layton JC, Foster PL. Error-prone DNA polymerase IV is controlled by the stress-response sigma factor, RpoS, in Escherichia coli. Mol Microbiol. 2003; 50:549–561. [PubMed: 14617178]
37. Sassanfar M, Roberts JW. Nature of the SOS-inducing signal in Escherichia coli. The involvement of DNA replication. J Mol Biol. 1990; 212:79–96. [PubMed: 2108251]
38. Wegel E, et al. Imaging cellular structures in super-resolution with SIM, STED and Localisation Microscopy: A practical comparison. Sci Rep. 2016; 6 27290 [PubMed: 27264341]
39. Banaz N, Mäkelä J, Uphoff S. Choosing the right label for single-molecule tracking in live bacteria: side-by-side comparison of photoactivatable fluorescent protein and Halo tag dyes. J Phys Appl Phys. 2018; 52 064002
40. Moreau PL. Effects of overproduction of single-stranded DNA-binding protein on RecA protein-dependent processes in Escherichia coli. J Mol Biol. 1987; 194:621–634. [PubMed: 3309327]
41. Schmidt A, et al. The quantitative and condition-dependent Escherichia coli proteome. Nat Biotechnol. 2016; 34:104–110. [PubMed: 26641532]
42. Thliveris AT, Mount DW. Genetic identification of the DNA binding domain of Escherichia coli LexA protein. Proc Natl Acad Sci U S A. 1992; 89:4500–4504. [PubMed: 1584782]
43. Oertel-Buchheit P, Porte D, Schnarr M, Granger-Schnarr M. Isolation and characterization of LexA mutant repressors with enhanced DNA binding affinity. J Mol Biol. 1992; 225:609–620. [PubMed: 1602473]
44. Stracy M, et al. Transient non-specific DNA binding dominates the target search of bacterial DNA-binding proteins. Mol Cell. 2021; 81:1499–1514. e6 [PubMed: 33621478]
45. Giese KC, Michalowski CB, Little JW. RecA-Dependent Cleavage of LexA Dimers. J Mol Biol. 2008; 377:148. [PubMed: 18234215]
46. Little JW, Gellert M. The SOS regulatory system: Control of its state by the level of RecA protease. J Mol Biol. 1983; 167:791–808. [PubMed: 6410076]
47. Neher SB, Flynn JM, Sauer RT, Baker TA. Latent ClpX-recognition signals ensure LexA destruction after DNA damage. Genes Dev. 2003; 17:1084–1089. [PubMed: 12730132]
48. Olivares AO, Kotamarthi HC, Stein BJ, Sauer RT, Baker TA. Effect of directional pulling on mechanical protein degradation by ATP-dependent proteolytic machines. Proc Natl Acad Sci. 2017; 114:E6306–E6313. [PubMed: 28724722]
49. Ronen M, Rosenberg R, Shraiman BI, Alon U. Assigning numbers to the arrows: Parameterizing a gene regulation network by using accurate expression kinetics. Proc Natl Acad Sci. 2002; 99:10555–10560. [PubMed: 12145321]
50. Mohana-Borges R, et al. LexA repressor forms stable dimers in solution. The role of specific dna in tightening protein-protein interactions. J Biol Chem. 2000; 275:4708–4712. [PubMed: 10671501]
51. Butala M, et al. Interconversion between bound and free conformations of LexA orchestrates the bacterial SOS response. Nucleic Acids Res. 2011; 39:6546–6557. [PubMed: 21576225]
52. Culyba MJ, Kubiak JM, Mo CY, Goulian M, Kohli RM. Non-equilibrium repressor binding kinetics link DNA damage dose to transcriptional timing within the SOS gene network. PLOS Genet. 2018; 14 e1007405 [PubMed: 29856734]
53. O'Reilly EK, Kreuzer KN. Isolation of SOS constitutive mutants of Escherichia coli. J Bacteriol. 2004; 186:7149–7160. [PubMed: 15489426]
54. Shepley DP, Little JW. Mutant LexA proteins with specific defects in autodigestion. Proc Natl Acad Sci U S A. 1996; 93:11528–11533. [PubMed: 8876169]
55. Dri AM, Moreau PL. Control of the LexA regulon by pH: evidence for a reversible inactivation of the LexA repressor during the growth cycle of Escherichia coli. Mol Microbiol. 1994; 12:621–629. [PubMed: 7934886]
56. Schuldiner S, et al. Induction of SOS functions by alkaline intracellular pH in Escherichia coli. J Bacteriol. 1986; 168:936–939. [PubMed: 3096964]
57. Shee C, et al. Engineered proteins detect spontaneous DNA breakage in human and bacterial cells. eLife. 2013; 2 e01222 [PubMed: 24171103]
58. Cox MM, et al. The importance of repairing stalled replication forks. Nature. 2000; 404:37–41. [PubMed: 10716434]

59. Michel B, Sandler SJ. Replication Restart in Bacteria. J Bacteriol. 2017; 199
60. Mangiameli SM, Merrikh CN, Wiggins PA, Merrikh H. Transcription leads to pervasive replisome instability in bacteria. eLife. 2017; 6 e19848 [PubMed: 28092263]
61. Ghodke H, et al. Spatial and temporal organization of RecA in the Escherichia coli DNA-damage response. eLife. 2019; 8 e42761 [PubMed: 30717823]
62. Gynnå AH, Wiktor J, Leroy P, Elf J. RecA mediated homology search finds segregated sister locus in minutes after a double stranded break. bioRxiv. 2020; 2020.02.13.946996 doi: 10.1101/2020.02.13.946996
63. Brent R, Ptashne M. Mechanism of action of the lexA gene product. Proc Natl Acad Sci U S A. 1981; 78:4204–4208. [PubMed: 7027256]
64. Loewer A, Batchelor E, Gaglia G, Lahav G. Basal dynamics of p53 reveals transcriptionally attenuated pulses in cycling cells. Cell. 2010; 142:89–100. [PubMed: 20598361]
65. Xia J, et al. Bacteria-to-Human Protein Networks Reveal Origins of Endogenous DNA Damage. Cell. 2019; 176:127–143. e24 [PubMed: 30633903]
66. Fitzgerald DM, Hastings PJ, Rosenberg SM. Stress-Induced Mutagenesis: Implications in Cancer and Drug Resistance. Annu Rev Cancer Biol. 2017; 1:119–140. [PubMed: 29399660]
67. Marciano DC, et al. Negative feedback in genetic circuits confers evolutionary resilience and capacitance. Cell Rep. 2014; 7:1789–1795. [PubMed: 24910431]
68. Chia N, Golding I, Goldenfeld N. Lambda-prophage induction modeled as a cooperative failure mode of lytic repression. Phys Rev E Stat Nonlin Soft Matter Phys. 2009; 80 030901 [PubMed: 19905052]
69. Datsenko KA, Wanner BL. One-step inactivation of chromosomal genes in Escherichia coli K-12 using PCR products. Proc Natl Acad Sci. 2000; 97:6640–6645. [PubMed: 10829079]
70. Los GV, et al. HaloTag: a novel protein labeling technology for cell imaging and protein analysis. ACS Chem Biol. 2008; 3:373–382. [PubMed: 18533659]
71. Baba T, et al. Construction of Escherichia coli K-12 in-frame, single-gene knockout mutants: the Keio collection. Mol Syst Biol. 2006; 2 2006.0008
72. Zaslaver A, et al. A comprehensive library of fluorescent transcriptional reporters for Escherichia coli. Nat Methods. 2006; 3:623–628. [PubMed: 16862137]
73. Bryant JA, Sellars LE, Busby SJW, Lee DJ. Chromosome position effects on gene expression in Escherichia coli K-12. Nucleic Acids Res. 2014; 42:11383–11392. [PubMed: 25209233]
74. Cohen SE, et al. Roles for the transcription elongation factor NusA in both DNA repair and damage tolerance pathways in Escherichia coli. Proc Natl Acad Sci. 2010; 107:15517–15522. [PubMed: 20696893]
75. Ivanković S, Đermić D. DNA End Resection Controls the Balance between Homologous and Illegitimate Recombination in Escherichia coli. PLOS ONE. 2012; 7 e39030 [PubMed: 22720024]
76. Shurtleff BW, Ollivierre JN, Tehrani M, Walker GC, Beuning PJ. Steric Gate Variants of UmuC Confer UV Hypersensitivity on Escherichia coli. J Bacteriol. 2009; 191:4815–4823. [PubMed: 19482923]
77. Kovačič L, et al. Structural insight into LexA-RecA* interaction. Nucleic Acids Res. 2013; gkt744 doi: 10.1093/nar/gkt744
78. Grimm JB, et al. A general method to improve fluorophores for live-cell and single-molecule microscopy. Nat Methods. 2015; 12:244–250. [PubMed: 25599551]
79. Martens KJA, Bader AN, Baas S, Rieger B, Hohlbein J. Phasor based single-molecule localization microscopy in 3D (pSMLM-3D): An algorithm for MHz localization rates using standard CPUs. J Chem Phys. 2017; 148 123311
80. Crocker JC, Grier DG. Methods of Digital Video Microscopy for Colloidal Studies. J Colloid Interface Sci. 1996; 179:298–310.
81. Uphoff S, Sherratt DJ, Kapanidis AN. Visualizing protein-DNA interactions in live bacterial cells using photoactivated single-molecule tracking. J Vis Exp. 2014 e51177
82. Sliusarenko O, Heinritz J, Emonet T, Jacobs-Wagner C. High-throughput, subpixel precision analysis of bacterial morphogenesis and intracellular spatio-temporal dynamics. Mol Microbiol. 2011; 80:612–627. [PubMed: 21414037]

83. Stylianidou S, Brennan C, Nissen SB, Kuwada NJ, Wiggins PA. SuperSegger: robust image segmentation, analysis and lineage tracking of bacterial cells. Mol Microbiol. 2016; 102:690–700. [PubMed: 27569113]

84. Stracy M, et al. Single-molecule imaging of UvrA and UvrB recruitment to DNA lesions in living Escherichia coli. Nat Commun. 2016; 7 12568 [PubMed: 27562541]

Europe PMC Funders Author Manuscripts

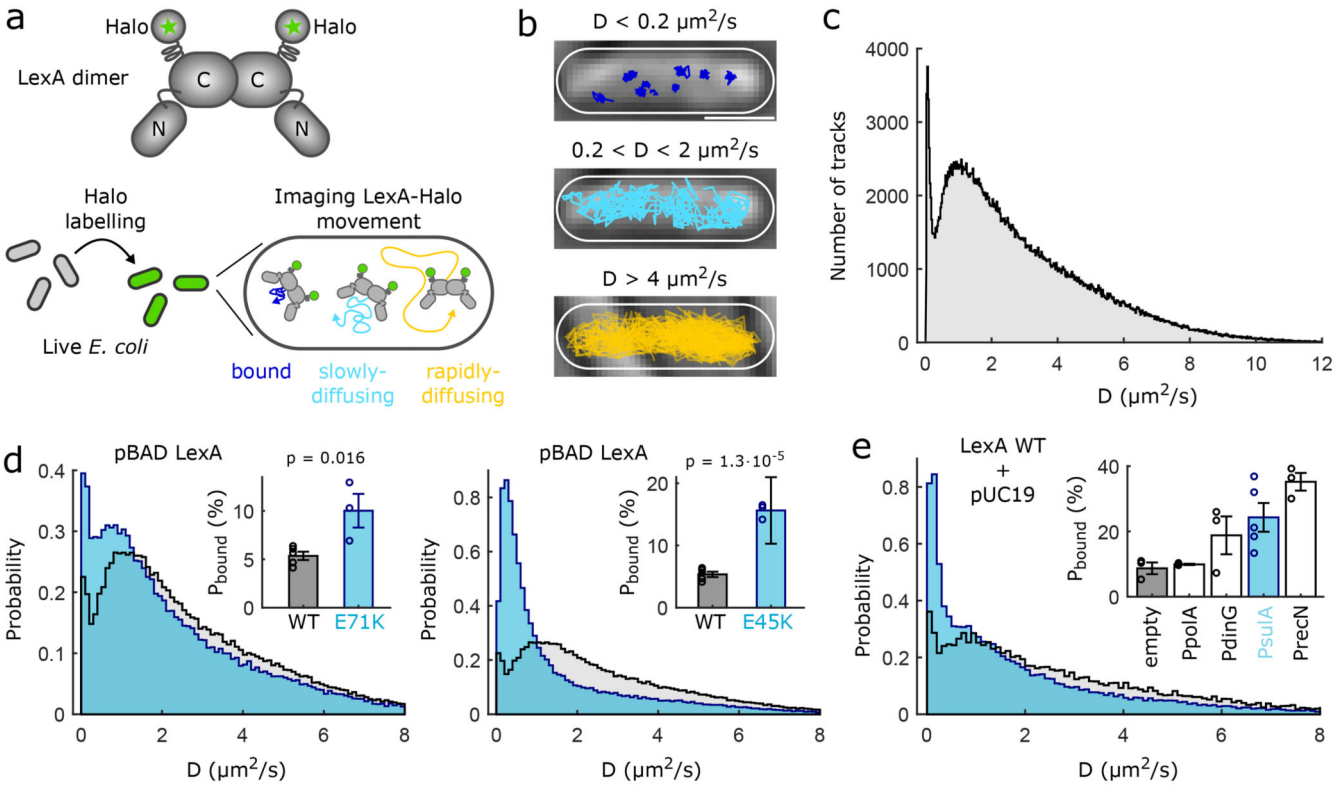

Fig. 1. Live-cell single-molecule tracking of LexA repressor.

a, Schematic of LexA-Halo tracking approach. **b,** Transmitted light image of an example cell with LexA-Halo tracks coloured according to the diffusion coefficient per molecule. **c,** D distribution of LexA-Halo in untreated wild-type cells (9 repeats, 2528 cells, 384241 tracks). **d,** D distributions for pBAD-expressed LexA-Halo mutants with increased DNA-binding affinity, E71K (blue, 3 repeats, 896 cells, 88432 tracks), E45K (blue, 3 repeats, 887 cells, 70496 tracks), compared to pBAD-expressed wild-type LexA-Halo (grey, 5 repeats, 1265 cells, 99306 tracks). Distributions are combined data from all repeats. Insets: Mean P_{bound} ± SEM with p-values from two-sided t-tests and individual measurements of biologically independent repeats. **e,** D distributions for wild-type LexA-Halo in cells carrying empty pUC19 plasmid (grey 3 repeats) or pUC19 with LexA-regulated promoter PsulA (blue, 5 repeats). Inset: Mean P_{bound} ± SEM and individual measurements of 3 biologically independent repeats for cells with empty pUC19 (314 cells, 15314 tracks), pUC19 with LexA-independent promoter PpolA (806 cells, 27747 tracks), pUC19 with SOS promoters PdinG (504 cells, 20636 tracks), PsulA (5 repeats, 822 cells, 46802 tracks), PrecN (659 cells, 35285 tracks). Scale bar: 1 μm.

Europe PMC Funders Author Manuscripts

Europe PMC Funders Author Manuscripts

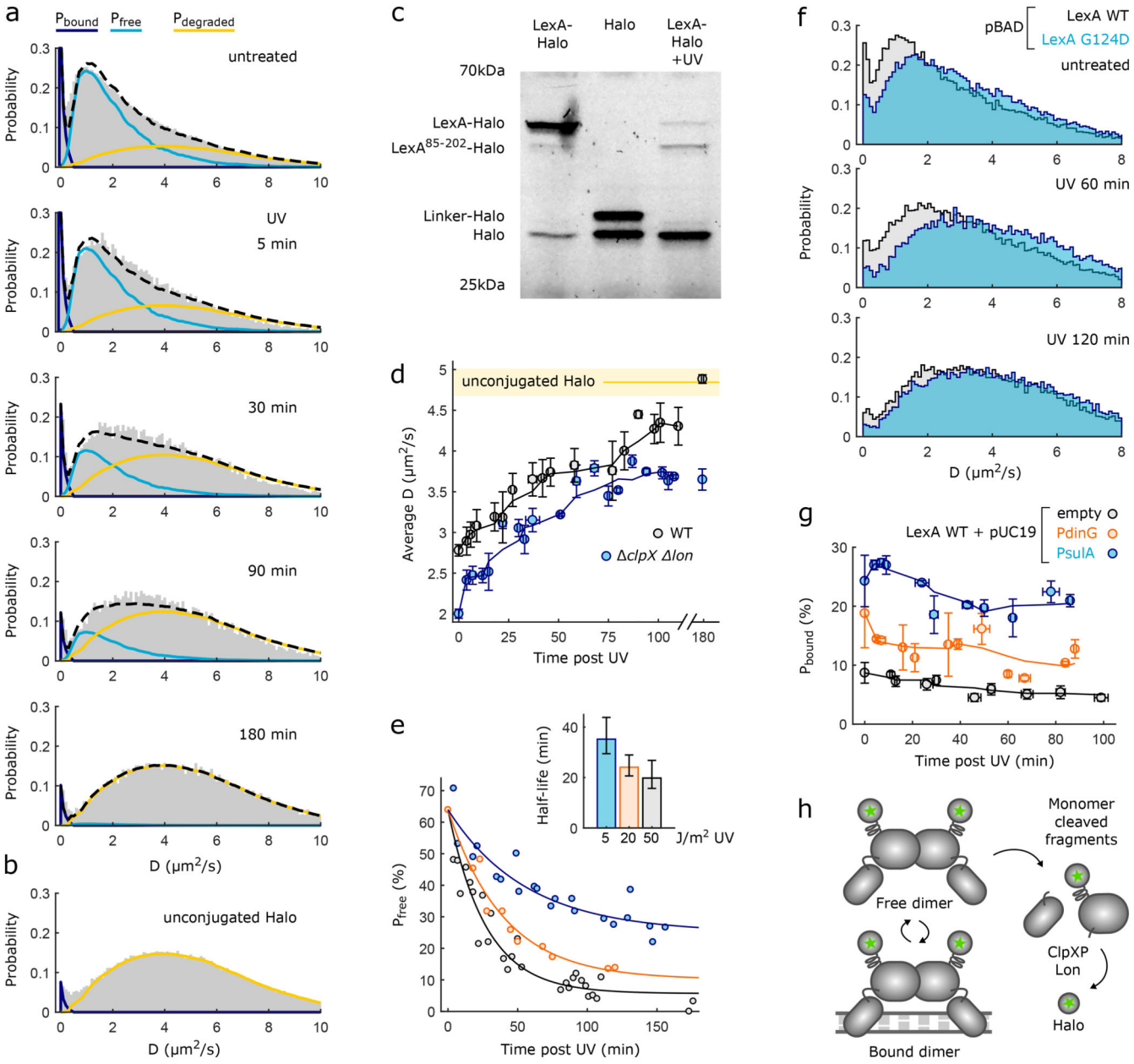

Fig. 2. Dynamics of LexA cleavage and degradation in response to DNA damage.

a, D distributions for LexA-Halo in untreated cells and at indicated times post 50 J/m^2 UV fitted with mixture model (dashed lines) of LexA populations P_{bound} (dark blue), P_{free} (light blue), $P_{degraded}$ (yellow). Combined data from 3 repeats per time point. Untreated: 9 repeats, 2528 cells, 384241 tracks. 5 min: 280 cells, 23452 tracks. 30 min: 295 cells, 15408 tracks. 90 min: 333 cells, 18338 tracks. 180 min: 307 cells, 18391 tracks. **b,** D distribution for unconjugated HaloTag expressed in untreated cells (3 repeats, 314 cells, 84763 tracks). **c,** SDS-PAGE ingel TMR fluorescence from cells expressing LexA-Halo, unconjugated HaloTag, LexA-Halo at 120 min post 50 J/m^2 UV exposure. The additional band for unconjugated HaloTag includes the protein linker. Representative gel from 3 biologically independent experiments. **d,** Average D of LexA-Halo after 50 J/m^2 UV in wild-type (black)

and Δ*clpX* Δ*lon* (blue) strains with moving average curves (error bars: SEM, N = 3 biologically independent experiments, average numbers per time point WT: 304 cells, 15365 tracks; Δ*clpX* Δ*lon*: 245 cells, 13216 tracks.). Average D ± SEM of unconjugated HaloTag in untreated cells shown for reference (N = 3, yellow line and shaded area). **e,** Decay of free LexA pool post UV exposure 5 J/m^2 (blue, 77 cells, 2986 tracks), 20 J/m^2 (orange, 44 cells, 2973 tracks), 50 J/m^2 (black, 84 cells, 6757 tracks). Average numbers per time point; 1 repeat per condition. Inset: decay half-life from exponential fits; error bars: 95% CI. **f,** D distributions for pBAD-expressed LexAG124D-Halo mutant and wild-type LexA-Halo from untreated cells (WT: 735 cells, 32583 tracks; G124D: 460 cells, 27215 tracks), after 50 J/m^2 UV at 60 min (WT: 595 cells, 30969 tracks; G124D: 736 cells, 13026 tracks) and 120 min (WT: 610 cells, 21528 tracks; G124D: 686 cells, 21724 tracks). Combined data from 3 repeats per time point. **g,** Decay of the bound LexA population post 50 J/m^2 UV exposure for cells carrying empty pUC19 plasmid, pUC19 with PdinG or PsulA (lines: moving average, error bars: SEM, N = 3 biologically independent experiments. Average numbers per time point: pUC19 empty: 232 cells, 5669 tracks; PdinG: 273 cells, 13186 tracks; PsulA: 290 cells, 18724 tracks) **h,** Schematic for SOS induction via LexA degradation.

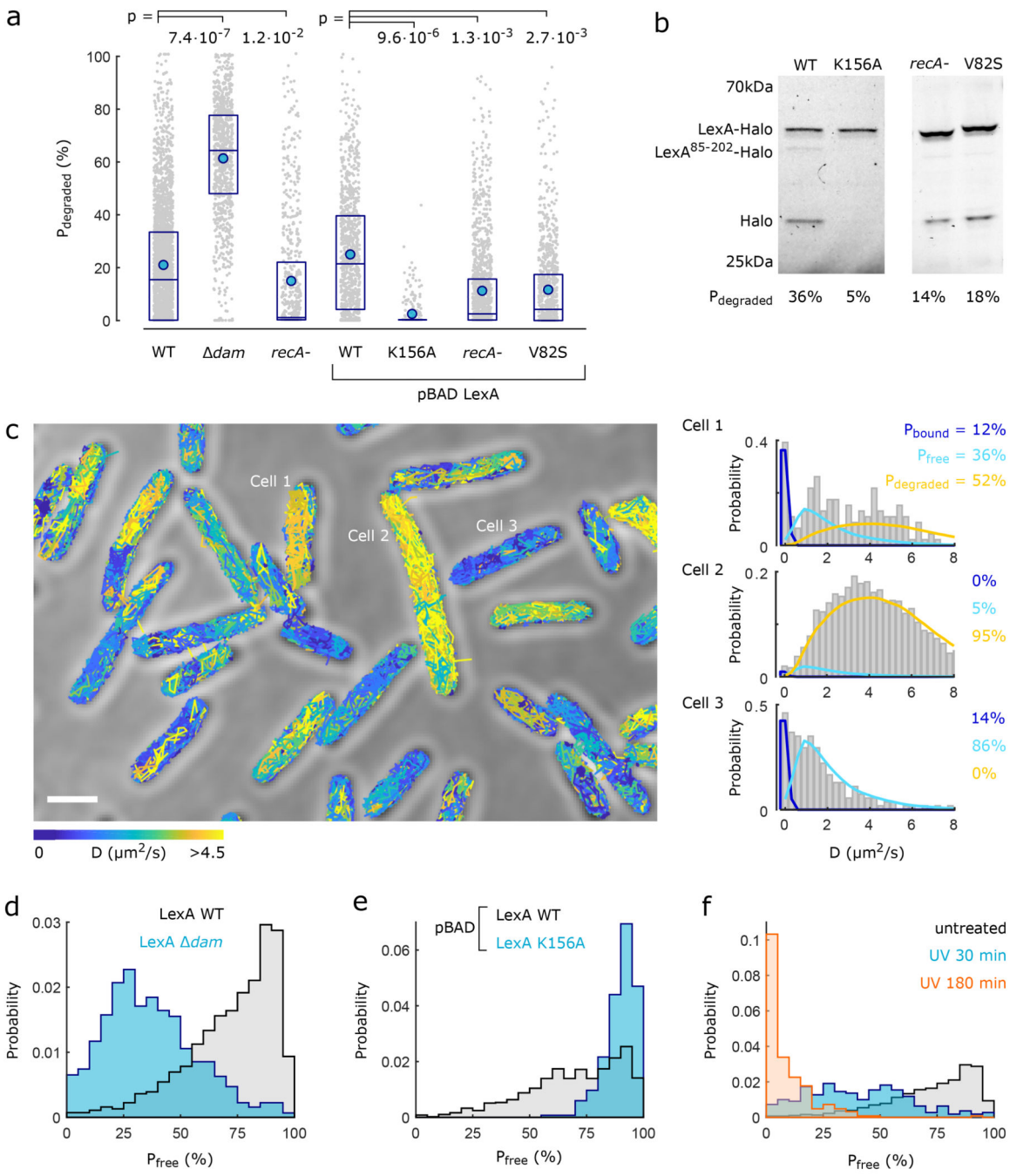

Fig. 3. Spontaneous LexA degradation in untreated cells is highly heterogeneous.

a, Abundance of degraded LexA-Halo population per cell in wild-type (14 repeats, 2756 cells), Δ*dam* (3 repeats, 889 cells), *recA*- (3 repeats, 640 cells) strains. pBAD-expressed wild-type LexA-Halo (5 repeats, 977 cells), LexAK156A-Halo (3 repeats, 268 cells), wild-type LexA-Halo in *recA*- strain (3 repeats, 1294 cells), LexAV82S-Halo (3 repeats, 916 cells). Boxes: 25-75% percentile, blue dots: averages, lines: medians, grey dots: individual cells, p-values from two-sided t-tests of biologically independent experiments. **b,** In-gel fluorescence from pBAD-expressed LexA-Halo wild-type, LexAK156A-Halo, LexA-Halo

Europe PMC Funders Author Manuscripts

wild-type in *recA*- strain, LexAV82S-Halo. Representative gels from 3 biologically independent experiments. **c,** Transmitted light image of untreated wild-type cells with LexA-Halo tracks coloured according to the diffusion coefficient per molecule. Scale bar: 2 μm. D distributions of example cells with mixture model for P_{bound}, P_{free}, $P_{degraded}$ populations. **d, e, f,** Abundance of free LexA-Halo population per cell for wild-type (14 repeats, 2756 cells), Δ*dam* strains (3 repeats, 889 cells), pBAD-expressed wild-type (5 repeats, 977 cells), LexAK156A-Halo (3 repeats, 268 cells), and for wild-type LexA-Halo at 30 min (3 repeats, 220 cells) and 180 min (3 repeats, 248 cells) post 50 J/m^2 UV.

Europe PMC Funders Author Manuscripts

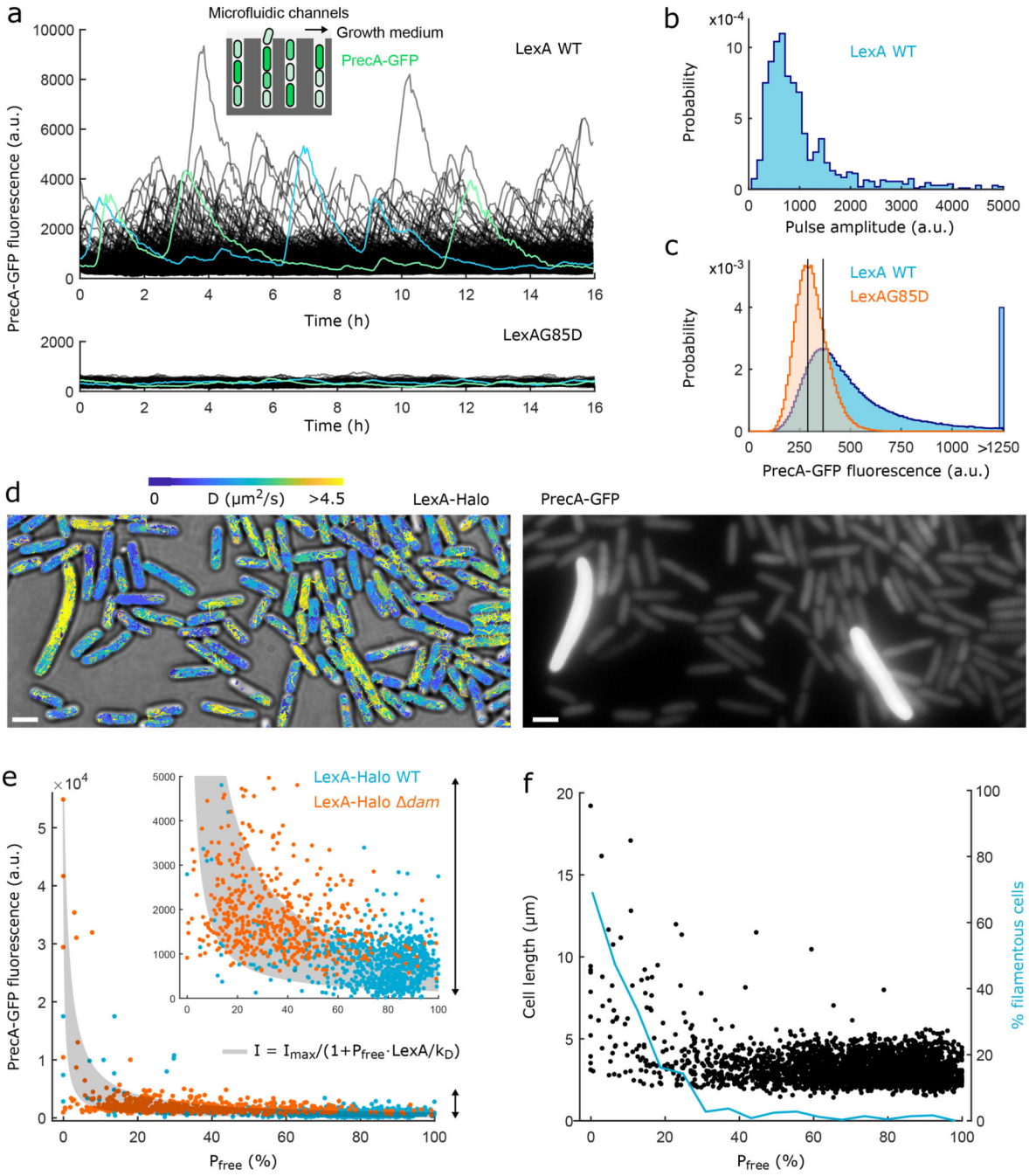

Fig. 4. Variability in LexA degradation underlies spontaneous SOS induction and expression heterogeneity.

a, Mothermachine microfluidic data showing single-cell dynamics of PrecA-GFP fluorescence for cells expressing wild-type LexA (3 repeats, 1095 cells), LexAG85D (2 repeats, 769 cells). Example cell traces highlighted. **b,** Distribution of PrecA-GFP pulse amplitudes (3 repeats, 1095 cells, 1136 pulses). **c,** Distributions of PrecA-GFP fluorescence for wild-type (3 repeats, 1095 cells) and LexAG85D (2 repeats, 774 cells) strains (vertical lines: distribution modes). **d,** LexA-Halo tracks on transmitted light image and PrecA-GFP

fluorescence in single cells. Scale bars: 2 μm. Representative image from 3 biologically independent experiments. **e,** PrecA-GFP versus free LexA abundance per cell for wild-type (blue dots, 3 repeats, 832 cells), Δ*dam* (orange dots, 3 repeats, 521 cells) strains. Grey area: Gene regulatory function for PrecA (I) controlled by P_{free} with total concentration of LexA dimers = 650 nM and PrecA affinity k_D between 2-10 nM. Inset: expanded section indicated by arrow. **f,** Left axis: Cell length versus free LexA abundance per cell (black dots, 9 repeats, 2504 cells). Right axis: Percentage of filamentous cells (length > 5μm) across a moving average of free LexA abundance per cell (blue line).